NUCLEAR HYPERFINE INTERACTIONS IN W^{182}, W^{183}, AND Pt^{195} AS STUDIED BY THE MOSSBAUER EFFECT

Thesis by
David G. Agresti

In Partial Fulfillment of the Requirements

For the Degree of
Doctor of Philosophy

California Institute of Technology
Pasadena, California
1967
(Submitted May 26, 1967)

ACKNOWLEDGMENTS

Many people have contributed to the progress of this work. In particular, the author would like to thank:

Dr. Egbert Kankeleit, who originally conceived and designed the experiments and provided needed guidance throughout all phases of the research.

Dr. Börje Persson, whose close collaboration made the completion of these studies possible.

Dr. Felix Boehm for his interest and support of these studies.

Dr. Rudolf Mössbauer for many helpful discussions on the solid-state aspects of the problem.

Dr. Edwin Seltzer for many illuminating discussions on nuclear theory and calculations of relevant nuclear parameters.

Mr. H. E. Henrikson for his help with the design of the experiment.

Dr. P. Duwez for his advice on metallurgical problems.

Dr. R. Willens for suggestions related to the levitation-melting technique.

Mr. Vagn Stephenson and Mr. Ellsworth "Woody" Kiersey for their help in making parts of the apparatus.

Mr. Granville "Glenn" Swanson for help with electronics.

Finally, Miss Jerre Levy Basch, with whom the author has had many pleasant discussions on the final wording of this thesis.

The author gratefully acknowledges financial aid from the California Institute of Technology, the U. S. Atomic Energy Commission, and the Woodrow Wilson Foundation.

ABSTRACT

The Mössbauer technique has been used to study the nuclear hyperfine interactions and lifetimes in W^{182} (2^+ state) and W^{183} ($3/2^-$ and $5/2^-$ states) with the following results: $g(5/2^-)/g(2^+) = 1.40 \pm 0.04$; $g(3/2^-) = -0.07 \pm 0.07$; $Q(5/2^-)/Q(2^+) = 0.94 \pm 0.04$; $T_{1/2}(3/2^-) = 0.184 \pm 0.005$ nsec; $T_{1/2}(5/2^-) \gtrsim 0.7$ nsec. These quantities are discussed in terms of a rotation-particle interaction in W^{183} due to Coriolis coupling. From the measured quantities and additional information on γ-ray transition intensities magnetic single-particle matrix elements are derived. It is inferred from these that the two effective g-factors, resulting from the Nilsson-model calculation of the single-particle matrix elements for the spin operators $\hat{s}_z$ and $\hat{s}_+$, are not equal, consistent with a proposal of Bochnacki and Ogaza.

The internal magnetic fields at the tungsten nucleus were determined for substitutional solid solutions of tungsten in iron, cobalt, and nickel. With $g(2^+) = 0.24$ the results are: $|H_{eff}(W\text{-}Fe)| = 715 \pm 10$ kG; $|H_{eff}(W\text{-}Co)| = 360 \pm 10$ kG; $|H_{eff}(W\text{-}Ni)| = 90 \pm 25$ kG. The electric field gradients at the tungsten nucleus were determined for WS_2 and WO_3. With $Q(2^+) = -1.81$ b the results are: for WS_2, $eq = -(1.86 \pm 0.05)\,10^{18}$ V/cm^2; for WO_3, $eq = (1.54 \pm 0.04)10^{18}$ V/cm^2 and $\eta = 0.63 \pm 0.02$.

The $5/2^-$ state of Pt^{195} has also been studied with the Mössbauer technique, and the g-factor of this state has been determined to be -0.41 ± 0.03. The following magnetic fields at the Pt nucleus were found: in an Fe lattice, 1.19 ± 0.04 MG; in a Co lattice, 0.86 ± 0.03 MG; and in a Ni lattice, 0.36 ± 0.04 MG. Isomeric shifts

have been detected in a number of compounds and alloys and have been interpreted to imply that the mean square radius of the Pt^{195} nucleus in the first-excited state is smaller than in the ground state.

To Jerre

From Jerre:

David does physics from morning till night--
From 8 in the evening till dawn's early light.
Energy spectra confuse and perplex--
No time for love and no time for sex.
Tungsten 182 and 183
Interest him more than music or me.
Magnetic dipoles, hyperfine interaction
Act upon Dave like magnetic attraction.

Typical people make love in the spring.
Typical robins and sparrows will sing.
Typical daisies and roses will bloom,
But if you know David, you shouldn't assume
That he is aware that it's spring and it's May.
His thesis is due and he works night and day.

However, I'm sure when he's post-PhD,
He'll remember there's May and remember there's me.

TABLE OF CONTENTS

LIST OF FIGURES

LIST OF TABLES

I. INTRODUCTION

I. INTRODUCTION

This thesis describes experiments performed over the past year and a half in which fundamental use has been made of a discovery made in 1957 by R. L. Mössbauer.[1] In essence Mössbauer's discovery demonstrated for the first time that certain γ-rays emitted from radioactive nuclei in solid matter have an energy resolution very nearly equal to that corresponding by the uncertainty principle to the lifetime of the nuclear state from which the γ-rays were emitted. This discovery meant an enormous improvement in the sharpness of such γ-rays, and several new avenues of research were opened up.

The experiments described in this thesis[2] utilized these very narrow γ-rays in order to investigate nuclear hyperfine interactions in a number of materials. Structure in the energy spectrum of these γ-rays, slight broadening, and small energy shifts, all previously obscured because of the poor resolution, could now be readily observed, and valuable information was gained about the nucleus and its interaction with its environment.

1) Origin of the Spectra

Previous to Mössbauer's work, the emission of γ-rays from nuclei was considered to be a process that could be understood without reference to the properties of the solid in which the nucleus was imbedded. That is, the energy spectrum of the γ-rays was supposed to depend only on the temperature of the material from which they were emitted but not on the fact that the emitting nuclei were bound together in a lattice. A free nucleus recoils after emission of a γ-ray and the energy of the γ-ray is reduced by an

amount, $E_o^2/2Mc^2$, where E_o is the energy of the γ-ray and M is the mass of the recoiling nucleus. The energy spectrum emitted from a collection of nuclei at temperature, T, is centered on this value, and has a Gaussian shape with width, $2\sigma = 2E_o\sqrt{kT/Mc^2}$.

If the nuclei are in a solid, the above conclusion holds only if the recoiling nucleus has sufficient energy to be dislodged from its lattice site. If not, lattice vibrations will be induced, and the shape of the emission spectrum will depend on the shape of the phonon spectrum of the host solid. If the free-atom recoil energy is less than the mean phonon energy, the possibility arises that a certain significant fraction, the recoil-free fraction f, of γ-ray emissions will not excite any phonon at all and will thus carry the full energy difference between the two nuclear levels involved in the transition. If both of these levels are degenerate, and the width of the energy spectrum is due to the finite lifetime, τ, of the upper state, then the emission spectrum will be given by the Breit-Wigner formula (Lorentzian line shape),

$$p(e) \propto \frac{1}{\left[1 + \frac{4}{\Gamma^2}(e - E_o)^2\right]}, \qquad (I.1)$$

where

$$\Gamma = \hbar/\tau = 0.693\hbar/T_{1/2}, \qquad (I.2)$$

and E_o is the transition energy. If one or both of the levels is shifted or is split into a number of sublevels by interaction of the nucleus with its surroundings, the emission spectrum will take the form of a sum over Lorentzian line shapes, with the relative contribution of each Lorentzian depending on the relative emission probabilities for the different energies of the γ-rays connecting the sublevels. Namely,

$$p'(e) \propto \sum_j \frac{h(j)}{\left[1 + \frac{4}{\Gamma(j)^2}\,(e - E(j))^2\right]} \quad . \qquad (I.3)$$

The parameters, E, h, and Γ, appearing in Formula I.3 contain valuable information about the nucleus and its environment, and the great value and interest in the Mössbauer effect arises because these quantities can be obtained from experiment. The energy spectrum for absorption of γ-rays by nuclei in a solid without energy transfer to the lattice has exactly the same form as the emission spectrum, Equation I.1 or I.3, as appropriate.

The thing that makes the Mössbauer effect so beautiful and so useful is that the emission (or absorption) spectrum may be modulated in energy by the experimenter as he desires. He does this by moving the source of γ-rays in a controlled and predetermined fashion; for example, if the source is moved in the direction of emission of γ-rays with velocity, v, then the emission spectrum is shifted toward higher energies by an amount, vE_o/c. He then records the number of γ-rays that pass thru the absorber for various velocities of the source both toward ($v > 0$) and receding from ($v < 0$) the absorber. The counting rate will fall when there is large absorption ($v \approx 0$) and rise when there is no absorption ($v \gg c\Gamma/E_o$). In particular, if the absorption spectrum, $p_a(e)$, is given by Equation I.3 and the emission spectrum, $p_s(e)$, by Equation I.1, then the experimental, or transmission, spectrum will be

$$P(v) = \int de \cdot\, p_s\left(e + \frac{vE_o}{c}\right) p_a'(e)$$

$$\propto \sum_j \frac{h(j)}{1 + \frac{4}{(\Gamma_s + \Gamma_a(j))^2}\left[\frac{vE_o}{c} - (E_a(j) - E_o)\right]^2} \quad . \qquad (I.4)$$

By analyzing his data in an appropriate manner, the experimenter will be able to obtain all the $\Gamma_a(j)$ and the $E_a(j)$ to within an additive constant and all the $h(j)$. Of course, the resolution will be too bad to obtain these quantities with any precision unless $\Gamma_s + \Gamma_a \lesssim |E_a(i) - E_a(j)|$ for all i and j. However, the resolution can be much worse than this and one can still obtain accurate values for the peak positions provided a way can be found to relate the various $E_a(j)$, such as assuming magnetic dipole or electric quadrupole hyperfine interaction.

There are two important restrictions on the transition that may be studied by this method, and these limit the number to extremely few cases, considering the total number of nuclear transitions. First, since an absorber is involved, the lower level must be reasonably long lived. In practice this means the ground state of a stable nuclide. Also, the absolute maximum change in counting rate is the recoil-free fraction of the source f_s, so that f must be at least a percent or two for an effect to be observable. This limits the transitions to energies of around 150 keV or less. The cross section, σ_o, for absorption by the resonant isotope of γ-rays having the proper energy is

$$\sigma_o = \frac{h^2c^2}{2\pi} \frac{1}{E_o^2} \frac{2I_{ex} + 1}{2I_{gd} + 1} \frac{1}{1 + \alpha} \frac{1}{1 + \beta} . \qquad (I.5)$$

In this formula, I_{ex} and I_{gd} are the excited- and ground-state spins, resp., α is the total electron conversion coefficient, and β includes all other processes available for de-excitation of the excited level, such as cascade via an intermediate level. For the absorber the mass absorption coefficient for zero-phonon processes is

$$\frac{1}{t_m} = f_a \sigma_o \frac{N_o}{A} a . \qquad (I.6)$$

Here, A is the molecular weight of each molecule of the absorber, a is the fraction, by weight, of resonant isotopes, and N_o is Avogadro's number.

2) Interpretation of the Spectra

For the experiments reported on in this thesis we have chosen 5 transitions in 3 nuclei; the nuclear level schemes are shown in Figure I. 1. In order to obtain information about the nucleus and its environment, we have studied the shape of transmission spectra taken with various sources and absorbers. Four mechanisms that affect the shape of the observed velocity spectra have been important for the present work. These are:

a) Line broadening. Each component line of the spectrum is expected to have a minimum width of $2\Gamma c/E_o$. This is never realized in practice. First of all, the generally non-negligible thickness, t, of the absorber results in a broadening according to Visscher's formula by an amount

$$\Delta v = 0.135 \frac{2\Gamma c}{E_o} \frac{t}{t_m} . \qquad (I.7)$$

However, for $t \lesssim 5t_m$, the distortion from Lorentzian line shape is not significant. Unresolved hyperfine splitting is also generally present and contributes to line broadening but the shape is frequently unaffected for practical purposes. Instabilities in the drive or the mechanical mounting of the source and the absorber

can sometimes also cause line broadening. A special effect, which we have had to consider in the experiment on the 47-keV level in W^{183}, is a broadening that occurs when the absorber is a powder and the size of the grains is $\gtrsim \frac{1}{5} t_m$. More will be said about this in Section III. 5.

b) Centroid shift. This may be caused in several ways, such as by second-order Doppler shift or by gravitational effects. Only the isomeric, or chemical, shift is important for us here. From the formula,

$$\text{I.S.} = \frac{2\pi}{3} Ze^2 [|\psi_a(0)|^2 - |\psi_s(0)|^2][R_{ex}^2 - R_{gd}^2], \qquad \text{(I.8)}$$

we see that for an isomeric shift to result, two conditions must be met: 1) the mean-square nuclear radii R in the excited and ground states must be different; and 2) the electronic charge density $|\psi(0)|^2$ at the site of the nucleus must be different in the source and the absorber. With this type of interaction, every component line of the spectrum is shifted by exactly the same amount as given by Equation I. 8.

c) Magnetic hyperfine interaction. This is the interaction between the nuclear magnetic moment, $\vec{\mu}$, and the effective magnetic field, $\vec{H}$, at the nucleus, which may arise from the electrons in the solid or be externally applied by the experimenter. It has the Hamiltonian,

$$\mathcal{H}_M = -\vec{\mu} \cdot \vec{H} = -g\mu_n \vec{I} \cdot \vec{H} \ , \qquad \text{(I.9)}$$

and the eigenvalues,

$$E_m = -g\mu_n Hm \ , \qquad \text{(I.10)}$$

where g is the nuclear g-factor, μ_n the nuclear magneton, and m = I, I - 1, ..., -I, is the magnetic quantum number. The interaction results in a splitting of the nuclear levels if $I \neq 0$ and resolved lines in the observed velocity spectrum if $2\Gamma \lesssim g\mu_n H$. Resolved lines result because the energy difference between the excited state and the ground state is no longer unique, but has the discrete set of values,

$$E_{mm'} = E_o - g'\mu_n Hm' + g\mu_n Hm \ , \qquad \text{(I.11)}$$

where the primes refer to the excited state and m and m' run over all possible values.

Each of the $(2I + 1) \times (2I' + 1)$ lines in the magnetic hyperfine spectrum has a corresponding relative intensity that may be determined from the theory of radiative transitions. If the two states with spins I and I' are connected by radiation of multipolarity, L, then a photon has the probability,

$$P_{mm'}(\theta) \propto \left\{ \begin{matrix} I & I' & L \\ m & -m' & \Delta m \end{matrix} \right\}^2 Z^{L}_{\Delta m}(\theta), \qquad \text{(I.12)}$$

of being emitted or absorbed at any angle, θ, relative to the quantization axis (direction of $\vec{H}$) in the transition between the substates, (I, m) and (I', m'). In the formula, $\left\{ \ \right\}$ is Wigner's 3j symbol, and Z has the following dependence on θ:

$$Z_0^1(\theta) = 1 - \cos^2\theta \qquad \text{(I.13a)}$$

$$Z_{\pm 1}^1(\theta) = \frac{1}{2} + \frac{1}{2}\cos^2\theta \qquad \text{(I.13b)}$$

$$Z_0^2(\theta) = 2\cos^2\theta - 2\cos^4\theta \qquad \text{(I.13c)}$$

$$Z_{\pm 1}^2(\theta) = \frac{1}{3} - \cos^2\theta + \frac{4}{3}\cos^4\theta \qquad \text{(I.13d)}$$

$$Z_{\pm 2}^2(\theta) = \frac{1}{3} - \frac{1}{3}\cos^4\theta \ . \qquad \text{(I.13e)}$$

These are the radiation patterns appropriate for dipole and quadrupole radiation, and have been drawn in Figure I. 2 for convenience.

By using a ferromagnetic source or absorber and an external field of suffucient strength to polarize them, the experimenter can control the direction of the photon relative to the quantization axis. For example, application of a strong longitudinal field fixes $\theta = 0^o$, while a field applied transverse to the photon direction requires that $\theta = 90^o$. Single crystal sources or absorbers also restrict the value of θ. If an unpolarized powder or polycrystalline source or absorber is used in which the grains are randomly oriented, then all values of θ are possible, and Formula (I. 12) reduces to

$$P_{mm'} \propto \left\{ \begin{matrix} I & I' & L \\ m & -m' & \Delta m \end{matrix} \right\}^2 . \qquad \text{(I.14)}$$

d) Electric quadrupole interaction. This is the interaction between the nuclear electric quadrupole moment, Q_{ij}, and the gradient of the electric field, $\nabla \vec{E} = -\nabla\nabla V$, at the site of the

nucleus, which is due to a nonspherical distribution of electric charge surrounding the nucleus. It has the Hamiltonian,

$$\mathcal{H} = -\frac{1}{6}\sum_{ij} Q_{ij}\,(\nabla_i E_j)_{nuc}. \qquad (I.15)$$

The electric field gradient is a second rank tensor, but can always be brought to diagonal form by choosing the proper set of three mutually perpendicular axes, fixed relative to the crystalline axes, to correspond to the ij of (I.15); furthermore, because of Laplace's equation, $\sum_i V_{ii} = 0$, only two of the V_{ii} are independent. It is customary to define

$$eq = V_{zz}, \quad \text{the magnitude of the electric field gradient,}$$

and

$$\eta = \frac{V_{xx} - V_{yy}}{V_{zz}}, \quad \text{the asymmetry parameter,}$$

where the axes have been chosen so that $|V_{zz}| \geq |V_{yy}| \geq |V_{xx}|$, in which case, $0 \leq \eta \leq 1$. With these definitions and the conventional definition of the nuclear electric quadrupole moment eQ, the Hamiltonian takes the form,

$$\mathcal{H}_Q = \frac{e^2qQ}{4I(2I-1)}\left\{\left[3\hat{I}_z^2 - I(I+1)\right] + \left[\frac{\eta}{2}\left(\hat{I}_+^2 + \hat{I}_-^2\right)\right]\right\} \qquad (I.16)$$

where

$$\hat{I}_\pm = \hat{I}_x \pm i\hat{I}_y .$$

If $\eta = 0$ the eigenvalues and eigenstates are obtained by inspection from Equation I. 16. Each substate (except the one with m = 0) is doubly degenerate and is specified by $\pm m$. However, when $\eta \neq 0$, $\mathcal{H}_Q$ does not commute with $\mathcal{H}_M$, the magnetic quantum numbers are no longer valid quantum numbers for the substates, and one must solve the secular equation for $\mathcal{H}_Q$ separately for each different value of I. In the present experiments, only the 2+ level of W^{182} and the 5/2-level of W^{183} showed measurable electric quadrupole interaction. The solutions for the secular equations for these two values of spin are presented in Table III. 4. The relative intensities of the transitions that result in these two cases are also presented in the table.

Figure I. 1

Partial nuclear level schemes for W^{182}, W^{183}, and Pt^{195}. Vertical arrows indicate the Mössbauer transitions. For W^{183} the symbols K = 1/2 and K = 3/2 refer to the two lowest bands.

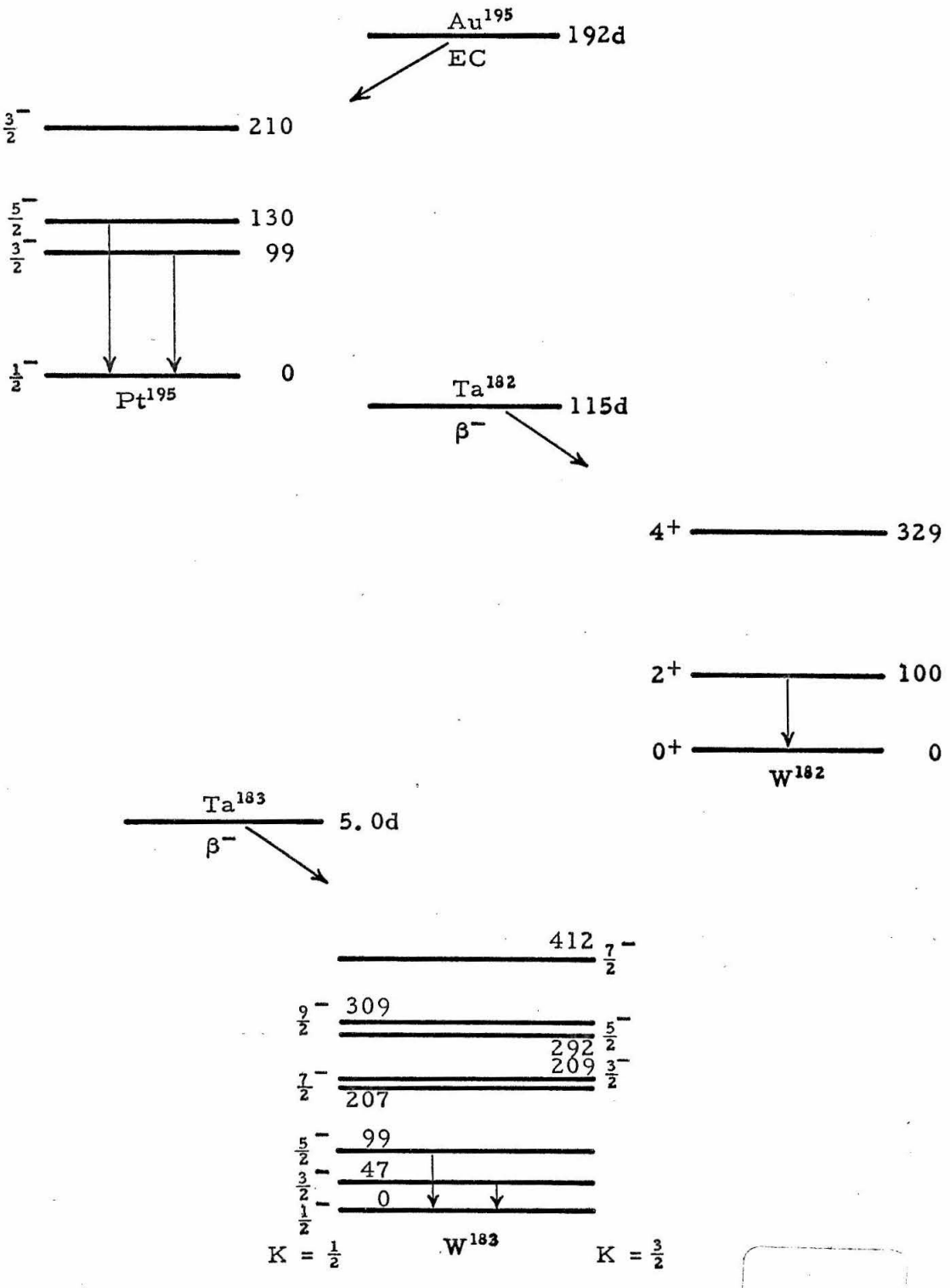
Au195
192d
EC
3/2− 210
5/2− 130
3/2− 99
1/2− 0
Pt195
Ta182
115d
β−
4+ 329
2+ 100
0+ 0
W182
Ta183
5.0d
β−
412 7/2−
9/2− 309
5/2−
292
209 3/2−
7/2− 207
5/2− 99
3/2− 47
1/2− 0
K = 1/2
W183
K = 3/2

Figure I. 1

Figure I.2

Dipole and quadrupole radiation patterns $Z^{L}_{\Delta m}(\theta)$.

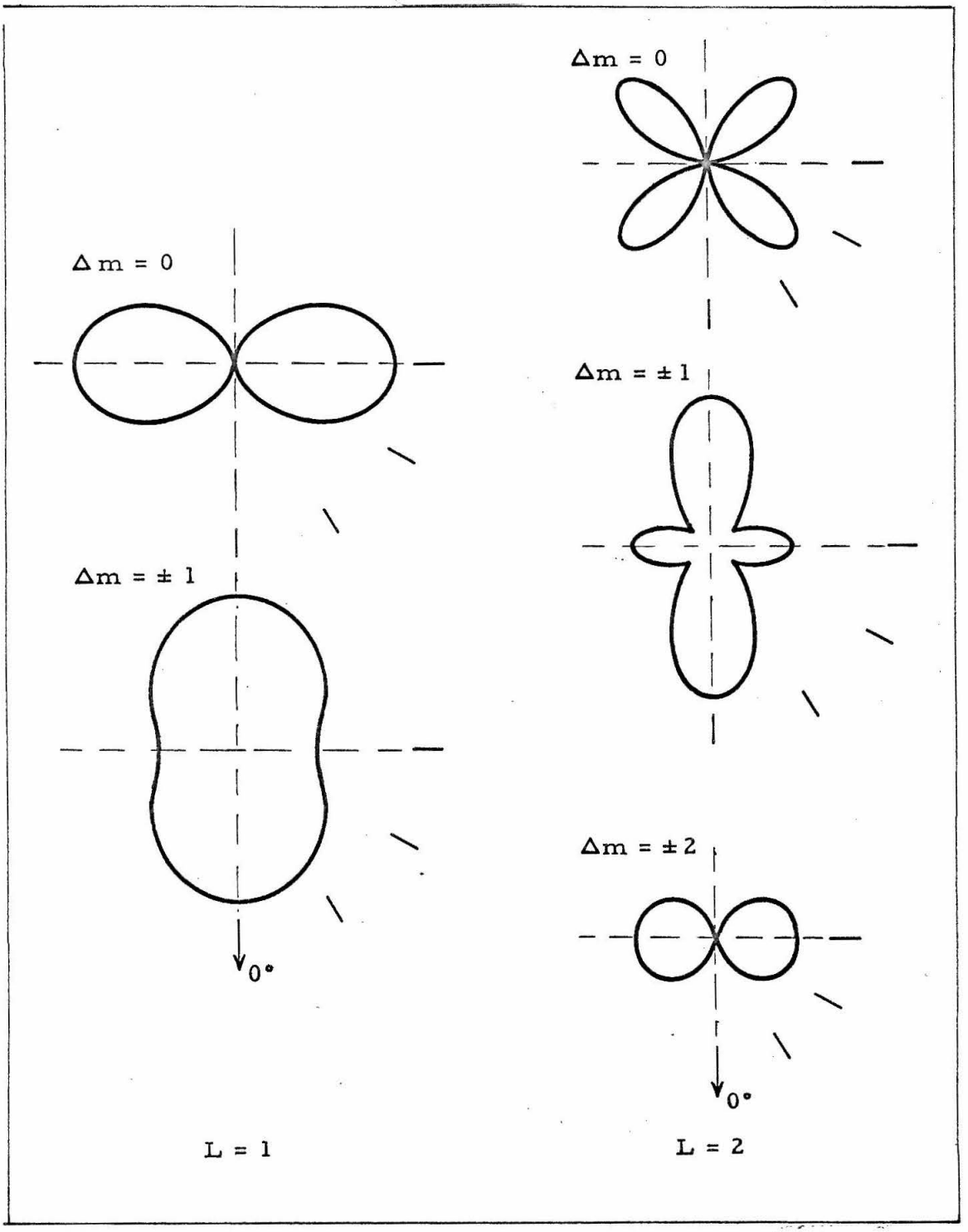

Figure I. 2

II. EXPERIMENT

II. EXPERIMENT

This chapter will describe the equipment and the materials used in the performance of the Mössbauer experiment. There are certain general aspects that practically all Mössbauer experiments have in common. These are:

1) A source of γ-radiation, generally produced by bombardment of stable nuclei with energetic particles, such as neutrons, protons, electrons, etc. The source may be used in the reactor during or just after production, or at a later date.

2) A detector, sensitive to the γ-rays of interest and equipped with a discriminator for selecting pulses due to those γ-rays.

3) An absorber or a scatterer, placed in the path of the γ-rays. When Mössbauer absorption takes place, the counting rate decreases in the detector discriminator if an absorber is used since the absorbed photons are removed from the beam and increases with a scatterer, because the detector is excited by photons emitted from the absorbing nuclei in the scatterer.

4) A drive, which moves the source or the absorber in a controlled and predictable fashion.

5) Recording equipment, which keeps a record of the number of pulses (γ-rays) appearing in the detector discriminator when the source or absorber is moving at a certain velocity. This record is the velocity spectrum (Figures III. 1-5, 7-9) and is analyzed numerically to obtain the information sought from the experiment.

All of these features are present in the experiments described in this thesis. However, in our experiments, only absorbers have been used, and the drive motion has been imparted to the source. Other equipment used in our experiments include a specially constructed cryostat for cooling the source and the absorber and magnets for polarizing the absorbers.

1) Sources and Detectors

As mentioned in the introduction (cf. Figure I. 1), we are concerned here with five transitions in the three nuclei W^{182}, W^{183}, and Pt^{195}. Extensive experiments were performed in only four of these, however, since the velocity spectrum for the fifth, the 130-keV of Pt^{195}, could barely be distinguished from the background after 40 hours of counting.

Sources for the W^{182} and W^{183} measurements were made by irradiating tantalum metal in a neutron flux of $3.3 \cdot 10^{14}$ n/cm^2 sec at the Materials Testing Reactor in Arco, Idaho. Since irradiation of natural Ta produces both Ta^{182} and Ta^{183}, and since the 100-keV line from the decay of Ta^{182} and the 99-keV line from the Ta^{183} decay cannot be separated by scintillation spectrometers (cf. Figure II. 1), precautions had to be taken to avoid a simultaneous measurement of recoiless absorption in W^{182} and W^{183}. For the W^{182} experiments a 10-mil wire of Ta was used as source since this was available from previous experiments on Ta^{182} with the bent-crystal monochrometer at Caltech and since the Ta^{183} (5.0 days) had had sufficient time to decay completely. The absorbers were made with unenriched tungsten.

For the W^{183} experiments the sources were 4-mil Ta foils especially irradiated for the present experiments. After arrival from the reactor they were checked with a lithium-drifted germanium detector to determine the relative intensities of the 99 and 100-keV γ radiation (from Ta^{183} and Ta^{182}, resp.). Since some of the higher energy peaks of Ta^{183} were easily resolvable from those of Ta^{182}, and since the intensity ratios of these peaks to the 99 and 100-keV peaks, resp., have been previously determined,[3] the relative intensities of the 99 and the 100-keV peaks could be calculated. It was found that only about 0.015 γ-ray of 100-keV energy (Ta^{182}) was emitted for every 99-keV γ-ray (Ta^{183}) at the time the source was removed from the reactor. However, the absorption coefficient (cf. Equation I. 6) for resonant absorption by unenriched tungsten absorbers is 7.3 times[3a] as great for the 100-keV γ-ray as for the 99-keV γ-ray, and enrichment of the absorbers in W^{183} was necessary to reduce the W^{182} contribution to the velocity spectra to a negligible amount. Because of the short lifetime of Ta^{183} the time during which the source could be used was limited to about two weeks after removal from the reactor, since at the end of this time the W^{182} contribution had grown to nearly 2% of the effect.

The source for the Pt^{195} experiments was commercially prepared and was 2 mCi of Au^{195} activity diffused into a 1-mil Pt foil.

A sodium iodide scintillation detector (1-1/2" x 1") and a double-delay-line amplifier were used to detect the γ-rays at a high counting rate. Since the detector was mounted close to the source and a superconducting solenoid (see Section II. 4) was used for longitudinal polarization of the absorbers, it was necessary to

compensate for the strong stray field ($\approx$ 0.5 kG) produced by the solenoid in order to avoid the use of a light guide which would have decreased the resolution of the scintillation detector. This was accomplished simply by surrounding the photomultiplier with a μ-metal mantle and a compensating coil. Adequate compensation could be provided, and almost the same resolution was obtained as in the absence of the stray field. The window of the single-channel analyzer, set for the relevant photopeak, contained about 50% background from other lines for the 100-keV transition in W^{182} and about 80%, 85%, and 35% for the 99-keV (W^{183}), 46.5-keV (W^{183}), and 99-keV (Pt^{195}) transitions, respectively (see Figure II. 1). The 47-keV line was enhanced by the use of a critical absorber of 180 mg/cm^2 Tb_4O_7. The precise position of the 47-keV photopeak was determined by recording the difference between pulse-height spectra obtained with and without recoiless absorption, i. e., with the source stationary and with the source oscillating with high velocity.

All source material was mounted in a holder like the one shown in Figure II. 2. The tubular end of the holder fits firmly onto a rod that extends from the drive (as in Figure II. 3). Working with solid or powdered source material is made much easier with this design, since the material can be placed into the cap and the body screwed down tightly. When sufficient precautions are taken, the outside of the holder does not become contaminated and the material is completely and rigidly held in place.

2) Absorbers

For the W^{182} and W^{183} experiments the absorber material used included W metal, the compounds WO_3, WS_2, and alloys of W with Fe, Co, and Ni. As pointed out in the previous section it proved necessary to use enriched materials for all the experiments performed with the 99-keV radiation of W^{183}. The enriched tungsten was obtained as $W^{183}O_3$, (82.5% W^{183}, 6.4% W^{182}), and thus all the absorbers for the W^{183} experiments had to be produced with the oxide as starting material. Since the nuclear moments of the 99-keV state were obtained as ratios to the moments of the 100-keV state, the absorbers for the W^{182} experiments had to be made in the same way, but with unenriched WO_3 as starting material.

Absorbers of tungsten metal powder used tungsten produced by the reduction of WO_3 in a hydrogen atmosphere at 850°C. Tungsten sulfide, WS_2, was made by fusing a stoichiometric mixture of tungsten (produced as above) and sulphur in a pure nitrogen atmosphere in a sealed quartz tube at 900°C. Experiments on W^{182} were also done with commercially obtained W and WS_2. The velocity spectra obtained for the two types of tungsten showed no significant difference, but the spectra for the two types of WS_2 were in total disagreement, in spite of the fact that their x-ray diffraction patterns were identical. (Compare Figures III. 7 and 8 and see Section III. 3a for further discussion.)

The alloy absorbers for both W^{182} and W^{183} contained 1.8 at. % tungsten dissolved in ultrapure iron, cobalt, and nickel, except for the tungsten-iron absorbers used for the measurements on the 46.5-keV transition, which contained 3.6 at. % tungsten.

(It was verified by Mössbauer experiments in W^{182} that the effective fields were the same for the two concentrations of tungsten.) The alloys were prepared by pressing tungsten powder (enriched for experiments on the 99-keV level, natural for W^{182}) into a small cavity in a pellet of the host material. By the use of the high-frequency field of a 5-kW induction furnace the pellet was levitated on a water-cooled silver boat and melted in an argon atmosphere. Then the melt was kept for around 5 minutes at a few hundred degrees above the melting point to homogenize it. The alloy was shaped by repeated rolling and tempering in hydrogen to obtain disc-shaped absorbers, which were used mainly for measurements with transverse applied fields. For measurements without applied field and with longitudinal field the absorbers were usually prepared by grinding the tempered alloy on a fine india stone and dispersing the powder (average grain size: 3.5μ) in molten wax. However, this was not possible for the absorbers used with the 99-keV radiation of W^{183}, since one of the disadvantages of making absorber material starting from enriched material is that it is prohibitively expensive to obtain large amounts of the material. It was thus difficult to grind the W^{183}-Fe alloy with the small amount of material available, and it was therefore necessary to use the disc-shaped absorber for the experiment with no applied field. Only partial polarization was achieved however, as is evident from the velocity spectrum (Figure III.3). Several experiments were also done with tungsten-iron alloy produced by another technique. It was prepared by arc-melting in an argon atmosphere and carefully annealing in hydrogen and resulted in a slightly smaller effective field than the material produced with the induction furnace (see Table III.2).

The Pt^{195} experiments used absorbers of Pt metal, the commercially obtained compounds Pt O, $Pt O_2$, $Pt Cl_2$, $Pt Cl_4$, and alloys of Pt with Al, Au, Fe, Co, and Ni. Most of the alloy absorbers were prepared similarly to the W-alloy absorbers by high-frequency melting, rolling, and tempering. A Pt-Fe alloy was prepared by arc-melting and carefully annealing for several days, but no change in the velocity spectra was observed for the two absorber preparations.

All of the alloys for both the W and the Pt experiments were carefully checked by x-ray analysis, and it was verified that they were all solid solutions except for the Pt-Al alloy. In this case the x-ray analysis indicated intermetallic-compound formation, which is to be expected since a solid solution at room temperature can be acquired only by extremely rapid quenching. [5)]

The absorbers were generally in one of three forms: solid plates or discs, powder dispersed in wax and shaped in a pill press to form a pellet, or powder held fixed in a plastic container. Tungsten and all the compounds were powdered absorbers, while Pt and the alloys were generally plates. Various reasons dictated the choice of the form of the absorber. For example, Pt is supplied as a foil; flat plates were used for the alloys with Fe, Co, and Ni to facilitate transverse polarization; on the other hand, for measurements without applied field powdered absorbers were used since this ensures that the orientation of domains is random. For convenience all powdered absorbers were in the form of wax pellets except those for the 99-keV experiments on W^{183}. The $W^{183}O_3$ and the W^{183} powders were held rigid in disc-shaped plastic containers rather than being mixed with wax for economic reasons. After the experiments were performed the powders were recovered for use in making WS_2 or W-alloy.

3) Drive and Data Storage

The motion of the source was provided by synchronizing the motion of a transducer with a multichannel analyzer operating in the multiscalar mode, as has been described in detail elsewhere.[6] The transducer provided a velocity of triangular waveform to within 0.3%, as determined from the error signal. The electromechanical drive was calibrated by measuring the velocity spectrum of a single-line Co^{57} source versus an absorber of Fe^{57} in Armco iron. An additional confirmation of the linearity of the velocity waveform was provided by taking calibration spectra at several different settings of the peak-to-peak velocity. Calibration spectra were measured with the source at 300, 77, and 4.2°K and the absorber at room temperature. The relative positions of the lines were those of Preston et al.,[7] which were used as the standard, to better than 0.4%. The data stored in the analyzer were punched onto paper tape, which was then converted into IBM cards for use with the computer program that analyzed the data.

4) Special Equipment

Because of the high energies of the transitions investigated, cooling of both the source and absorber is required to obtain a measureable resonant absorption except for the 47-keV experiments. Most of the experiments were therefore performed at liquid-helium temperature in a cryostat as shown in Figure II. 3. The cryostat consists basically of two coaxial cylindrical containers separated by an evacuated volume (10^{-7} - 10^{-6} torr). The outer container is made from an aluminum tube and the inner one from thin (7-mil) stainless-steel sheet. The inner one is wrapped with about forty layers of "super-insulation", a submicron glass paper

alternating with layers of 1/2-mil aluminum foil. Each layer of aluminum foil is separately connected to the inner container above the helium level so that the outer foils are connected to the upper warmer part of the container. With this arrangement the heat content of the outgoing gas is efficiently used. At the top of the cryostat is placed a set of thin stainless-steel plates, which serve the double purpose of radiation shields and separators for a number of gas layers, thereby reducing the convection. These reflector plates and the filling tubes are mounted to the plate covering the top of the cryostat. A center hole in this assembly allows the extended part of the drive system, containing the source and the absorber, to be easily inserted into the cryostat. The transducer itself rests on the top plate outside the cryostat. The construction of the cryostat is simple and inexpensive, and a helium consumption of about 0.13 ℓ/h is generally achieved.

The transducer, the source, and the absorber are enclosed in a container that is easily removed from the cryostat. The lower extended part, the source tube, is made of thin-walled (10-mil) stainless steel. It is surrounded by the liquid helium, but is closed on the lower end by a thin beryllium disc which serves as a window for the γ-rays and allows the container to be evacuated and filled with an exchange gas for heat transfer. The drive motion is transmitted to the source by an extension rod (1/4" dia., 6-mil wall stainless-steel tube) which is centered by a spiral-shaped phosphor-bronze spring in the absorber holder, which is held firmly in place in the source tube by a stiff spring. By lifting off the cover to the drive container and pushing the exposed center tube of the drive (containing the drive coils) downward, the absorber holder is brought into the position where the centering spring is unextended.

A small carbon resistor mounted on the extension rod is used to monitor the temperature of the source and the absorber. The ease with which the source and absorber may be removed from the cryostat, changed and re-inserted allows the use of strong sources.

For the magnetization of the absorber in a direction transverse to the γ-ray beam, a C-shaped permanent magnet is used and is mounted to the outside of the source tube. It provides a field of about 2.5 kG in the plane of a disc-shaped absorber. Longitudinal magnetic fields of up to 50 kG at the absorber are supplied by a superconducting solenoid. Current leads to the coil and the heater for the superconducting switch are passed through a long thin-walled stainless-steel tube and end in four annular contact surfaces that mate with the solenoid contacts. It is important to avoid contamination of the contacts with films of solid air or ice since the increased contact resistance causes unnecessary heating which results in excessive helium loss during the charging of the coil. Current to the coil up to 30 amperes is supplied by a simple transistor circuit powered by storage batteries.

The velocity spectra for the experiments with the 100-keV radiation of W^{182} (Figure III. 1) demonstrate that the polarization of the absorber was just as expected: longitudinal, transverse, or random, as appropriate. We were thus assured that complete polarization or randomness was obtained in the absorbers used for the 99-keV experiments in W^{183} and Pt^{195} even though we were not able to verify this fact directly because of the poor resolution of the velocity spectra in these cases.

Figure II. 1

NaI(Tl) scintillation spectra for the Ta^{182}, Ta^{183}, and Au^{195} sources. The solid lines represent the full scintillation spectra, and the dashed lines the discriminated peaks. The hatched areas indicate the background included in the peaks. The number on the ordinate is a typical rate in the discriminated peak with the absorber in place.

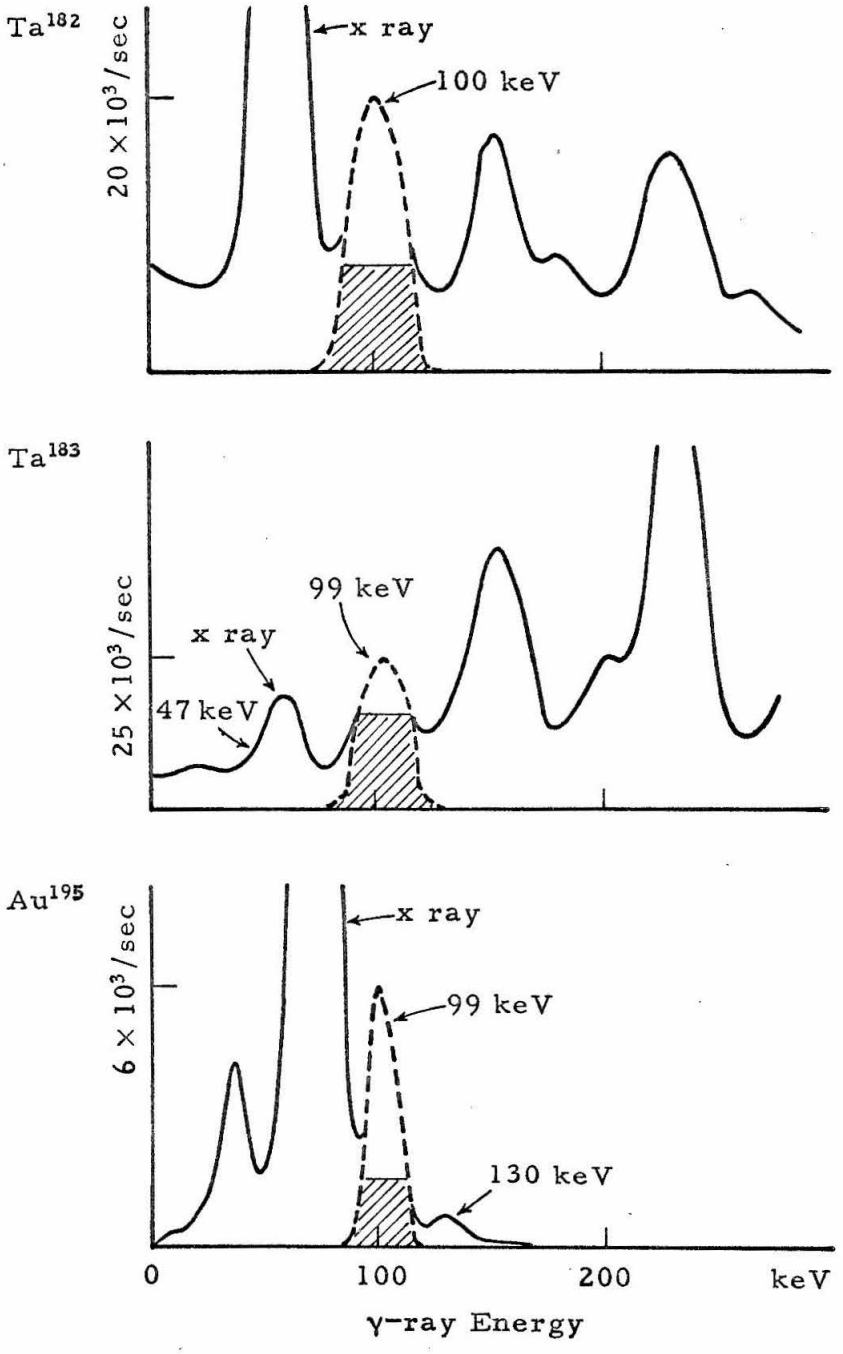
Ta182
20 × 10³/sec
x ray
100 keV
Ta183
25 × 10³/sec
99 keV
x ray
47 keV
Au195
6 × 10³/sec
x ray
99 keV
130 keV
0
100
200
keV
γ-ray Energy

Figure II. 1

Figure II. 2

Source holder. The source material is placed in the cap and the body is screwed down with wrenches fitted to the flats. The body is bored out to be fitted onto the drive extension rod, and the sides are slit to provide tension.

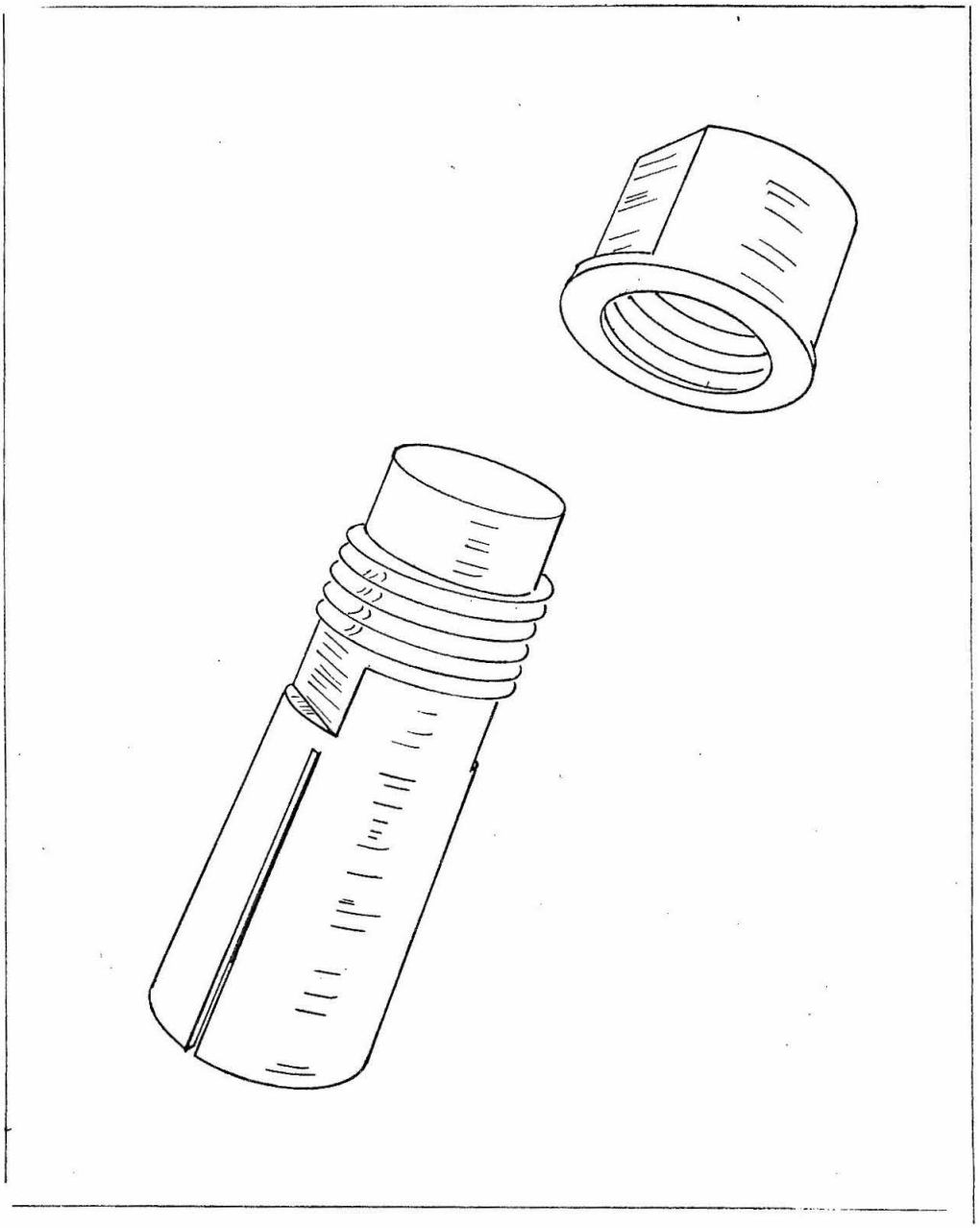

Figure II. 2

Figure II. 3

Schematic diagram of the cryostat and the drive system used in the experiment.

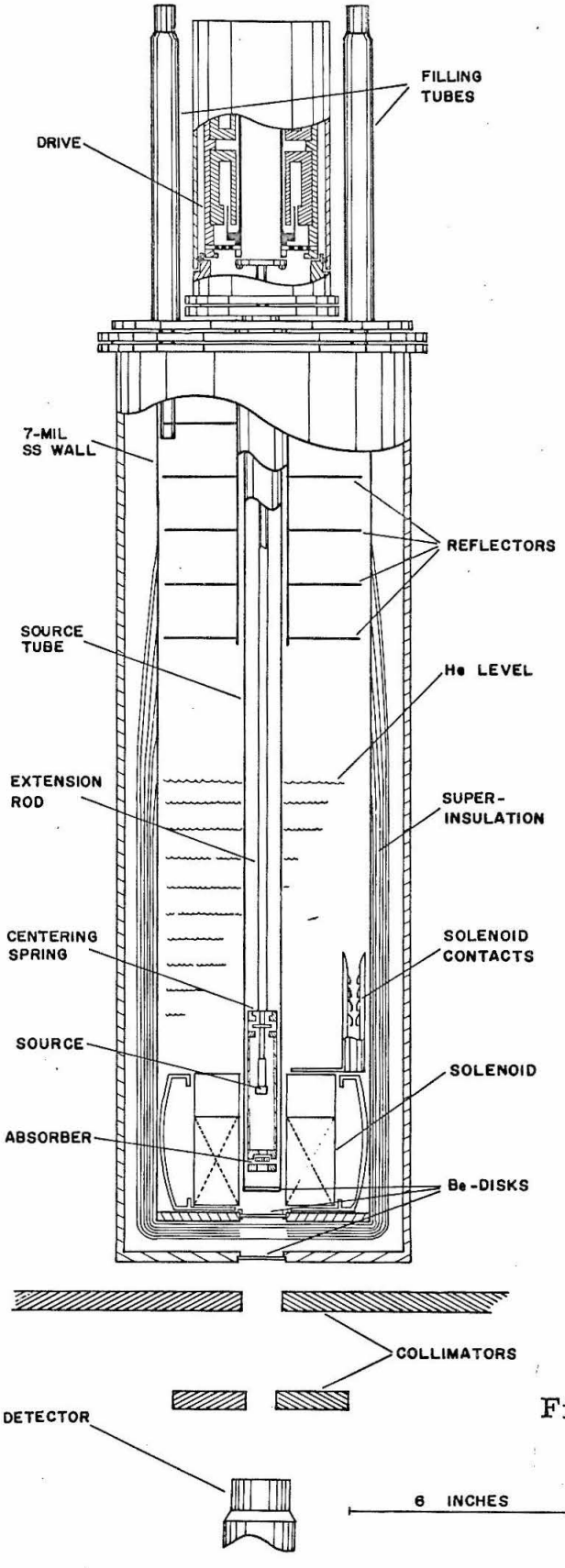
FILLING TUBES
DRIVE
7-MIL SS WALL
REFLECTORS
SOURCE TUBE
He LEVEL
EXTENSION ROD
SUPER-INSULATION
CENTERING SPRING
SOLENOID CONTACTS
SOURCE
SOLENOID
ABSORBER
Be-DISKS
COLLIMATORS
DETECTOR
6 INCHES

Figure II. 3

III. RESULTS

III. RESULTS

Shown in Figures III. 1-5, 7-9 are examples of velocity spectra illustrating the various experimental situations encountered. Partially resolved magnetic hyperfine spectra have been obtained for the 100-keV transition in W^{182}, the 99-keV in W^{183}, and the 99-keV in Pt^{195} (Figures III. 1-5), and have been used to obtain H_{eff} for W and Pt in Fe, Co, and Ni. The magnetic moments of the 99-keV levels in W^{183} and Pt^{195} have also been derived. Spectra with structure originating in electric quadrupole hyperfine interactions (Figures III. 7-9) have been used to obtain the ratio of electric quadrupole moments Q(2+)/Q(5/2-) for W^{182} and W^{183} and also the gradient of the electric field eq for WS_2 and eq and the asymmetry parameter η for WO_3. An isomeric shift has been identified for the first time in Pt^{195} (cf. Figures III. 4-6) and has yielded information about the first-excited and ground-state radii. An estimate has been made for the lifetime of the 99-keV state of W^{183}, but because unresolved broadening is present in the corresponding spectra, the error is quite large. The 47-keV transition of W^{183} is so broad that structure cannot be resolved. We have treated this case specially (cf. Figure III. 10) in order to obtain a value for the magnetic moment and the lifetime of the 47-keV state.

The spectra have been analyzed on the Caltech IBM 7094 computer by fitting them with the least-squares method to a sum of Lorentzian-shaped lines (Equation I. 4). The interpretation of the spectra is based on Section 2 of the Introduction, and the application to each particular case will be made as we discuss the analysis of each spectrum. A number of variable parameters determine the positions, intensities, and widths of the lines. These parameters

are: background B; slope of the background S; total dip of the spectrum (% effect) H; peak width w; center shift (Pt^{195} only) c; parameters used in specifying the peak positions e(j) when magnetic dipole or electric quadrupole interactions are present; and additional parameters used when it is desired to vary the relative intensities h(j) of the component peaks in the fitting procedure. The formula we used in fitting the spectra was based on Equation I. 4, and has the form

$$R(v) = B \cdot 10^6 \left\{ 1 + \frac{S}{10^2} \cdot v - \frac{H}{10^2} \sum_{j=1}^{N} \frac{h(j)}{1 + \frac{4}{w^2}\left[v - c - e(j) \right]^2} \right\} \quad \text{(III. 1)}$$

where v is the instantaneous velocity of the source, R is the counting rate in the detector, and N is the number of component peaks. The formula represents the sum of a slanted baseline and a number of Lorentzian peaks. The slanted baselines are thought to be caused by phase shifts in the pulse electronics. A spectrum was taken with a nonresonant absorber to verify that the baseline was linear. The h(j) are normalized by requiring $\Sigma\, h(j) = 1$.

Sometimes, and particularly for the Pt-Fe spectra of Pt^{195}, a considerably improved determination of essential parameters can be achieved by a combined fitting procedure in which several different spectra are analyzed together in one single least-squares procedure. A parameter in the function assigned to fit any one of the spectra might also be used in the functions for other spectra. An example of this is the line width corrected for absorber thickness. Therefore spectra measured under different but complementary conditions (e. g., applied magnetic fields) and fitted together usually determine a common parameter more precisely than the same spectra fitted

individually. If a combined fit of several spectra is possible, systematic errors might be revealed if present in one spectrum but not in the others.

1) Magnetic Hyperfine Interaction

For three transitions partially resolved magnetic hyperfine interaction was observed: the (2^+-0^+) 100-keV of W^{182}, the $(5/2^--1/2^-)$ 99-keV of W^{183}, and the $(3/2^--1/2^-)$ 99-keV of Pt^{195}. These spectra are shown in Figures III. 1-5. In each case the heavy solid line that runs through the experimental points is the fitted spectrum, and the lighter, smaller curves are the Lorentzian peaks that contribute to the resultant spectrum. The positions of the component peaks and their relative intensities are determined in accordance with the rules described in Section I. 2c.

Formula (I. 11) gives the general relation used in fitting the peak positions; it is used in the following form:

$$E_{mm'} = E_o + g\mu_n H [m - (g'/g)m'] . \qquad \text{(III. 2)}$$

In this formula E_o represents the experimental centroid shift of the spectrum, $g\mu_n H$ is the splitting of the sublevels of the ground state, and g'/g is the ratio of the g-factor of the excited state to that of the ground state. Thus if $I \neq 0$ (as in W^{183} and Pt^{195}), the magnetic parameters to be varied in the fit are $g\mu_n H$ and g'/g. However if $I = 0$ (as in W^{182}), then

$$E_{mm'} = E_o - g'\mu_n H m' , \qquad \text{(III. 3)}$$

and the variable magnetic parameter is $g'\mu_n H$ only.

The relative intensities of the component peaks depend on the spins of the ground and the excited state, I and I', respectively, on the multipolarity of the radiation, L, and on the polarization of the absorber. For "No H_{ext}" (as used to designate the spectrum in the figures) formula (I. 14) holds. For "$\| H_{ext}$" or "$\perp H_{ext}$" formula (I. 12) must be evaluated. Table III. 1 gives the relative peak intensities obtained in this manner. Since the polarization of the absorber was known, the peak intensities were not allowed to vary from the values listed in the table.

a) $(2^+ - 0^+)$ 100-keV transition in W^{182}. The best resolved of the spectra obtained in this work are those of Figure III. 1. These are spectra measured with a Ta^{182} source and tungsten-iron absorbers in various field configurations. The quality of the fit in each case demonstrates that for "$\| H_{ext}$" and "$\perp H_{ext}$" complete alignment was achieved and for "No H_{ext}" the alignment was completely random. These spectra were also subjected to a combined fit (Results in Table III. 2) by restricting the magnetic parameter $g'\mu_n H$ as well as the widths of the individual Lorentzians to the same values for all spectra. Small corrections for the effect of the external fields on the splittings (for $\| H_{ext}$) and for the differences in the effective absorber thicknesses due to different spectrum shapes were taken into account. The combined fit gave results and errors not significantly different from the individual fits and thus served as further confirmation that the absorber polarization was as intended.

The internal field at the tungsten nucleus was determined by adopting the value $g(2^+) = 0.24$ for the g-factor of the 2^+ state, an average of several recent measurements,[8] and consistent with the value 0.25 calculated by Nilsson and Prior.[9]

In Figure III. 2 are shown spectra taken with absorbers of tungsten dilutely dissolved in cobalt and nickel. Since systematic errors affecting the polarization of the absorbers were found not to be present for the experiments on W dissolved in Fe, the measurements were performed only with transverse applied field. The peak heights were taken in the fit to be those appropriate to the transverse polarization. To obtain H_{eff} a value was adopted for $g(2^+)$, as above.

A check on the reliability of the fitted spectra when they are composed of a number of Lorentzian peaks is provided by comparing the width of each component peak with the width of an absorber without hyperfine interaction, in this case tungsten. By referring to Table III. 2, we see that the width of the component peaks in the magnetic hyperfine spectra agree well with that measured for a pure tungsten absorber, after correction for absorber thickness.

b) $(5/2^- - 1/2^-)$ 99-keV transition in W^{183}. The observed magnetic hyperfine patterns, shown in Figure III. 3 for a Ta^{183} source and enriched tungsten-iron absorbers in the various field configurations were subjected to a combined fit similar to that for the Ta^{182} spectra. However, since a disc-shaped solid absorber was used for the measurement without any applied field and an experiment with Ta^{182} and a solid absorber of similar shape indicated a partial magnetic alignment, a combined fit was also performed excluding this Ta^{183} measurement. (The results of these fits are included in Table III. 2.) For both types of combined fit, a determination of both the internal field and the g-factor of the $5/2^-$ state was attempted, but due to the strong correlation between the two parameters the fits were very little affected by a change in the value of either of them, and both parameters could not be accurately

determined from the Ta^{183} measurements alone. Therefore, the internal field was fixed at the value determined from the Ta^{182} measurements, and as a consequence the value obtained for $g(5/2^-)$ depends on the adopted g-factor of the 2^+ state in W^{182}. Our results have been computed on the basis of the combined fit that excluded the no-field measurement, because the partial magnetic alignment of the absorber in the absence of an applied field resulted in a poorer fit when this measurement was included. The ratio $g(5/2^-)/g(2^+) = 1.40 \pm 0.04$ is constant to well within the error for $g(2^+)$ within $0.2 < g(2^+) < 0.3$ and can be used to evaluate $g(5/2^-)$ when $g(2^+)$ has been consistently determined.

It is possible to fit the present measurements also with a negative g-factor for the excited state, as well as the positive value we have been considering so far. The fit is, however, not so good as with the positive value, and the width of the fitted Lorentzians agrees not so well with the width determined for a tungsten absorber (refer to Table III. 2). A negative g-factor can therefore be ruled out.

c) $(3/2^- - 1/2^-)$ 99-keV transition in Pt^{195}. The magnetic hyperfine patterns obtained for different field configurations and alloys of Pt with Fe, Co, and Ni are shown in Figures III. 4 and 5. The spectra show little structure, and the individual peaks are not resolved. But an isomeric shift is clearly observed for the alloys and will be discussed in the next section. The relative intensities of the peaks in the fits were taken to be those appropriate for a pure M1 transition.[10), 11)] Fits to the individual spectra revealed a strong correlation among four parameters, namely excited-state g-factor $g_{3/2}$, effective field H_{eff}, width w, and effect, i. e., dip of the absorption spectrum. A unique determination of these parameters

was therefore not possible. However, the situation was found to improve markedly when a simultaneous fit was performed to the spectra for all three field configurations. The parameters $g_{3/2}$, H_{eff}, isomeric shift (I.S.), and width corrected for the difference in the absorber thickness were constrained to be the same for the six sets of data we had to fit. As a consequence the strong correlations among the four parameters, i.e., the corresponding off-diagonal elements of the error correlation matrix, were reduced up to 50%, and unique and rather precise values can be quoted for these parameters. The results are presented in Table III.3. The result for $g_{3/2}$ is based on the value $g_{1/2} = 1.21204$.[12)]

As a check on the internal consistency among the individual measurements, drastically changed weights were assigned to them, and the simultaneous fits were repeated. The spread of the parameter values that resulted was compatible with the standard deviations. In fitting individual spectra minima for Q^2 could sometimes be obtained for different sets of parameters. With this in mind we repeated the simultaneous fit searching for other minima, but none was found.

Figure III.5 shows spectra from measurements with transverse applied field on Pt-Co and Pt-Ni absorbers. By constraining $g_{3/2}$ to the value obtained from the fit to the Pt-Fe data, H_{eff} could be determined for the other alloys. The results for the fits are presented in Table III.3.

2) Isomeric Shifts

a) W^{182} and W^{183}. No evidence for an isomeric shift has been found in the measurements reported here (upper limit: 0.05 mm/sec in W^{182}).

b) Pt^{195}, 99-keV. Isomeric shifts are clearly observed for Pt in Fe, Co, and Ni (see Figures III. 4 and 5). In addition to these alloys, shifts were measured also for 20 at. % Pt in Au and 0.7 at. % Pt in Al. The shifts are plotted in Figure III. 6 versus the electronegativity of the host metal. Isomeric shifts have also been observed in some compounds of Pt; namely, PtO (-0.34 ± 0.11 mm/s), PtO_2(-0.40 ± 0.08 mm/s), $PtCl_2$(-0.1 ± 0.2 mm/s), and $PtCl_4$(-0.3 ± 0.3 mm/s).

From Figure III. 6 it is seen that the isomeric shift for the alloys decreases linearly with decreasing electronegativity[13] of the host element. (Pt-Al should be disregarded since it was not a solid solution. Refer to Section II. 2). This trend is opposite to that observed for Au^{197} by Barret et al.[13a] If we adopt the line of reasoning that decreased electronegativity of the host material results in an increased electron density at the impurity nucleus, it follows that the mean square radius of the Pt^{195} nucleus in the first-excited state is smaller than that in the ground state.

3) Electric Quadrupole Interaction

Only the $(2^+ - 0^+)$ 100-keV transition of W^{182} and the $(5/2^- - 1/2^-)$ 99-keV transition of W^{183} yielded measurable electric quadrupole interaction. The observed spectra are shown in Figures III. 7-9. The positions of the component peaks in these spectra are given generally by Equation I. 16, since the ground states are unsplit by the quadrupole interaction. For I = 2 and I = 5/2 Table III. 4 gives the energy levels E resulting from the electric quadrupole interaction, the substates ψ, and the relative transition intensities T from the ground state expected for a polycrystalline absorber with randomly oriented crystallites. In the table e^2qQ is the electric quadrupole

splitting factor, and it was varied in the fitting of the spectra. For fitting WO_3 spectra, η was also variable. In several cases the relative peak heights given in the table did not provide a good fit, and were therefore allowed to vary.

a) $(2^+ - 0^+)$ 100-keV transition in W^{182}. The observed electric quadrupole patterns for the 100-keV transition in W^{182} are shown in Figures III.7 and 8. The analysis (results in Table III.5) of the tungsten disulfide spectra was performed with $\eta = 0$ since WS_2 is axially symmetric.[14] It was found that fixing the relative peak intensities at 2:2:1 (cf. Table III.4) did not give a good fit. They were therefore allowed to vary, and the fit improved. The analysis of the velocity spectrum for the interaction energy e^2qQ was found however, to be insensitive to the relative intensities.

Spectra were taken with absorbers of commercially obtained and laboratory prepared (see Section II.2) WS_2. The peak heights fit to the spectrum for the commercially obtained WS_2 deviated more strongly from the expected 2:2:1 ratio than the home prepared material, and the deviations of the peak heights for the two preparations were of opposite sign. X-ray and spectroscopic analysis showed no difference between the two materials. In view of the exceptionally high magnetic susceptibility of tungsten disulfide, the measurements on the commercial material were repeated at $1.5^{\circ}K$ with the absorber in a magnetic field of 50 kG to check on a possible magnetic interaction. No change in the anomalous spectrum was observed. At $77^{\circ}K$ a quadrupole pattern with peak intensities in the expected ratio of 2:2:1 was obtained (Figure III.8), which contradicts an explanation in terms of an anisotropic Debye-Waller factor.[15] So far, no explanation for this effect is available.

In view of the difficulties encountered in the study of the quadrupole interactions in tungsten disulfide, a similar study of tungstic oxide was performed to obtain an independent determination of the ratio of the quadrupole moments for W^{182} and W^{183}. The symmetry at the site of the tungsten nucleus in tungstic oxide is known to be low and implies a non-axially symmetric electric field gradient, i. e. $\eta \neq 0$, at the tungsten nucleus. As is demonstrated in Table III. 5 and Figure III. 7, a reasonable fit to the measured velocity spectrum for the transition in W^{182} requires a large asymmetry parameter, contradicting previous results.[16)]

b) $(5/2^- - 1/2^-)$ 99-keV transition in W^{183}. The velocity spectrum obtained for a Ta^{183} source and an absorber of enriched tungsten disulfide shows very little structure, as seen from Figure III. 9. Therefore, the analysis of this spectrum is not very sensitive to the relative intensities of the peaks. Since the compound was prepared by the same technique as that for the W^{182} measurement, the relative intensities of the lines were inferred from that measurement and were kept fixed in the least-squares fitting procedure. The parameters e^2qQ for W^{182} and W^{183} in WS_2 could therefore be directly compared and the ratio $Q(2^+)/Q(5/2^-)$ obtained. In fitting the velocity spectrum obtained with the WO_3 absorber, η was fixed and set equal to the value determined from the W^{182} experiment. The resulting ratio of the quadrupole moments is in good agreement with that determined from the tungsten disulfide experiments.

c) Pt^{195}, 99-keV. An attempt was made to observe an electric quadrupole hyperfine interaction with this transition.

Absorbers of $PtCl_2$, $PtCl_4$, PtO, and PtO_2 were used but no statistically significant quadrupole interaction was seen.

4) Line Widths

Each spectrum fitted is assumed to be one Lorentzian dip or a composition of several, all of the same width. For each transition studied the widths of component peaks of the composite spectra were not significantly different from the width obtained for the unsplit absorber when the broadening effects due to absorber thickness were taken into account. Because these widths matched the width of the unsplit absorber, our confidence in the correctness of the fits was increased. Factors contributing to the widths of the peaks are discussed in Section I. 2a.

a) W^{182}, 100-keV. The widths obtained from the various experiments on the $(2^+ - 0^+)$ transition in W^{182} are in good agreement with the width observed using a tungsten metal absorber. The mean of the experiments, corrected for absorber thickness is 2.30 ± 0.06 mm/sec. A smaller value for this width, 2.0 ± 0.2 mm/sec, has been quoted elsewhere.[17] The discrepancy might be due to source broadening and to some extent to noise produced by the boiling liquid.

b) W^{183}, 99-keV. As for W^{182}, there is good agreement among the widths determined for the $(5/2^- - 1/2^-)$ transition in W^{183}. These widths do not, however, correspond to the natural width, because of source broadening. After the decay of Ta^{183} the source was checked in a W^{182} experiment, and the width observed with an absorber of 20 mgW/cm^2 was 3.5 mm/sec. In spite of this broadening

the spectrum shape was practically Lorentzian; hence the analysis of the W^{183} (99-keV) spectra in terms of Lorentzian components is justified. One can estimate the lifetime of the $5/2^-$ state if one corrects for the source broadening by assuming it to be caused by distributed electric field gradients. Then the width is 3.9 ± 0.4 mm/sec, which corresponds to the half-life $T_{1/2}(5/2^-) = 0.72 \pm 0.07$ nsec.

c) Pt^{195}, 99-keV. The width, corrected for thickness broadening, taking an average over several of the experiments is 18.0 ± 0.3 mm/sec, which implies an lower limit for the lifetime of this state of $T_{1/2} \geq 0.154$ nsec. This agrees with the electronically measured lifetime of $T_{1/2} \leq 0.16$ nsec.[18)]

5) Special Case: 47-keV transition in W^{183}

A determination of the lifetime and the magnetic moment of the $3/2^-$ state in W^{183} was attempted. The dependence of the absorption spectrum on the thickness of tungsten metal and tungsten-iron alloy absorbers was studied. For absorbers of uniform thickness, the half width of the nearly Lorentzian velocity spectrum is expected to depend linearly on the thickness of the absorber[19)], and the width corresponding to zero thickness can be determined by linear extrapolation, as demonstrated in Figure III.10. Fine powder (average grain size ≈ 0.5 and ≈ 0.02 recoilless resonant absorption lengths for W and W-Fe, respectively) dispersed in wax was, however, used for the absorbers. It was found for the tungsten measurements that the widths measured are affected by the absorber granularity to the extent that Visscher's formula[19)] cannot be used to determine the

natural line width. The effects of absorber granularity have been treated in detail elsewhere.[20] The correction to the extrapolated width is approximately proportional to the grain size measured in units of the recoilless resonant absorption length (t_m of Equation I. 6). In Figure III. 10 estimations of this correction to the tungsten measurements are indicated, from which it is inferred that the corresponding correction to the tungsten-iron measurements is negligible due to the much smaller grain size.

To avoid granularity effects, and since sufficiently thin tungsten metal foils could not be obtained, solid absorbers of tungsten-nickel alloy were used for the determination of the natural line width of the 46.5-keV transition. Line broadening due to magnetic interaction is negligible. From a combined least-squares fit to the observed velocity spectra for six absorber thicknesses, restricting the fitted widths to be proportional to the thickness of the absorber, the width for zero absorber thickness was determined to be 32.0 ± 0.8 mm/sec, which corresponds to the half-life $T_{1/2}(3/2^-) = 0.184 \pm 0.005$ nsec. Similarly, the velocity spectra obtained for tungsten-iron absorbers were fitted in one least-squares procedure. The value 32.0 ± 0.8 mm/sec was taken for the width corresponding to zero absorber thickness, and the ground-state splitting was fixed to a value in accordance with the measured internal field. The magnetic moment of the $3/2^-$ state was then determined by the fit: $g(3/2^-) = -0.07 \pm 0.07$ or $g(3/2^-) = 0.2 \pm 0.2$. Only negative values for $g(3/2^-)$ are, however, consistent with other experimental quantities (cf. Section IV. 2) . A fit to the W-Fe data with variable width for zero absorber thickness was also possible and gave values in agreement with the above, but with somewhat larger errors.

Figure III.1

Recoilless resonant absorption spectra for the 0^+-2^+ transition (100 keV) in W^{182} for tungsten dilutely dissolved in iron. The spectra correspond to various magnetic alignments of the absorber relative to the γ-ray beam. The slightly slanted baselines are thought to be caused by phase shifts in the pulse electronics.

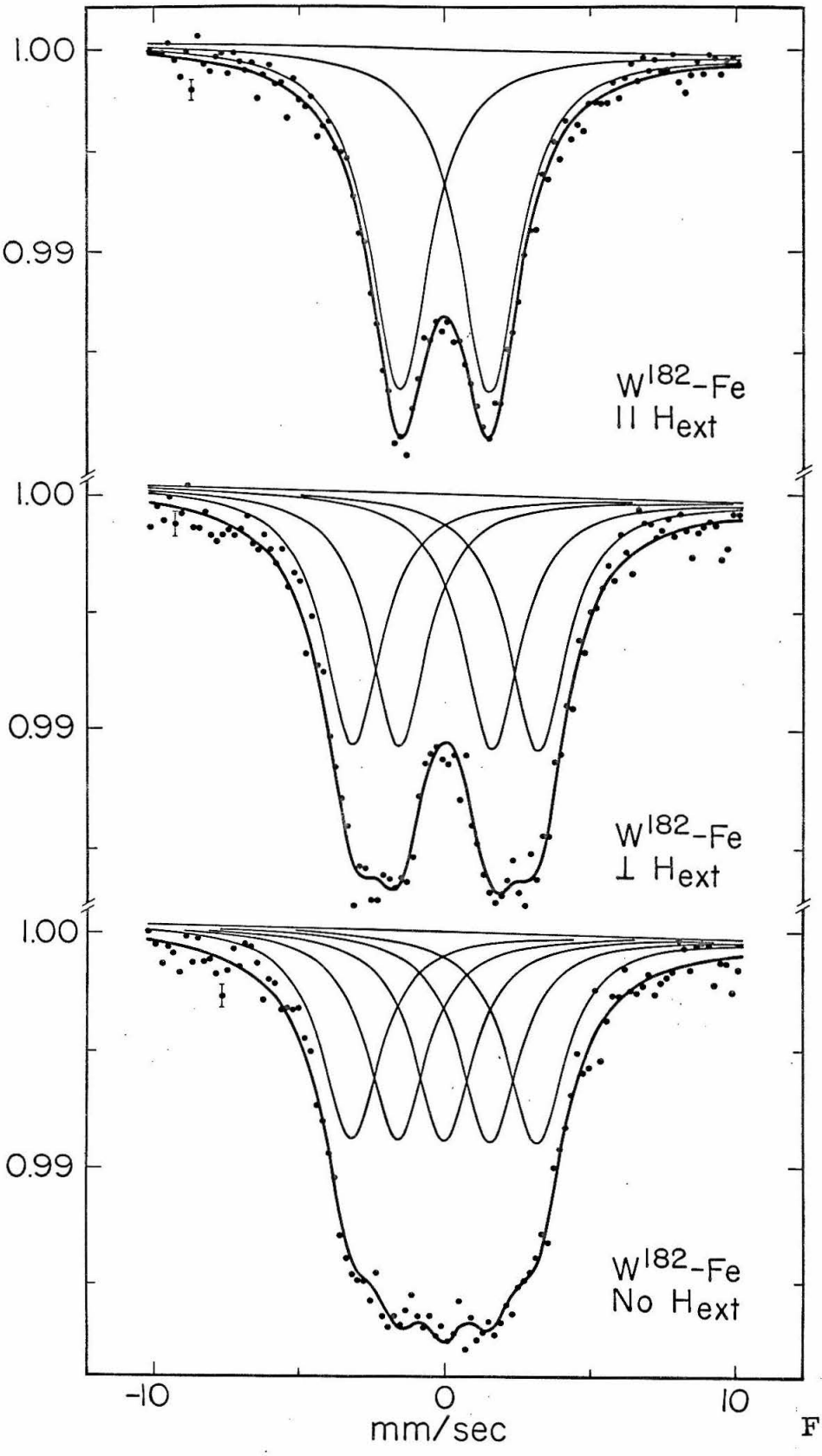
1.00
0.99
W182-Fe
II Hext
1.00
0.99
W182-Fe
⊥ Hext
1.00
0.99
W182-Fe
No Hext
-10
0
10
mm/sec

Figure III. 1

Figure III. 2

Recoilless resonant absorption spectra for the 0^+-2^+ transition in W^{182} for absorbers of tungsten dilutely dissolved in cobalt and nickel and of tungsten metal powder. The ferromagnetic absorbers were magnetized in a direction transverse to the γ-ray beam. The slightly asymmetric velocity pattern for W-Co may indicate presence of quadrupole interaction. A somewhat better fit to the spectrum was obtained assuming combined magnetic and quadrupole interaction. The quadrupole interaction may be appreciable, but it turns out that the value determined for the internal magnetic field is practically not affected.

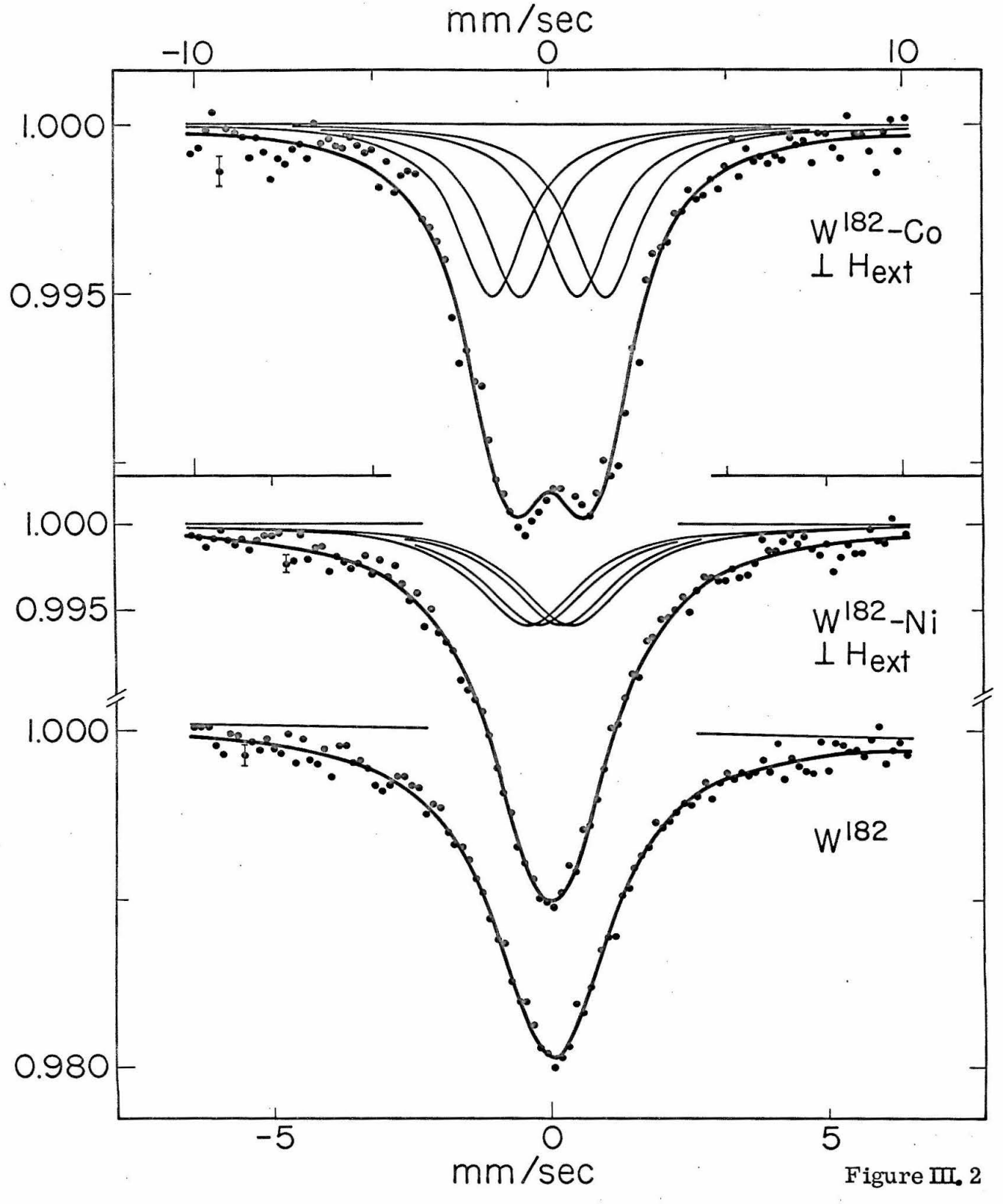
mm/sec
-10
0
10
1.000
0.995
W182-Co
⊥ Hext
1.000
0.995
W182-Ni
⊥ Hext
1.000
W182
0.980
-5
0
5
mm/sec

Figure III. 2

Figure III. 3

Recoilless resonant absorption spectra for the $1/2^- - 5/2^-$ transition (99 keV) in W^{183}. A disk-shaped absorber of enriched tungsten dilutely dissolved in iron was used. The solid curves are the fitted functions for the three spectra simultaneous fitted by the least-squares method. The dashed curves correspond to the fit to the two spectra measured with applied fields.

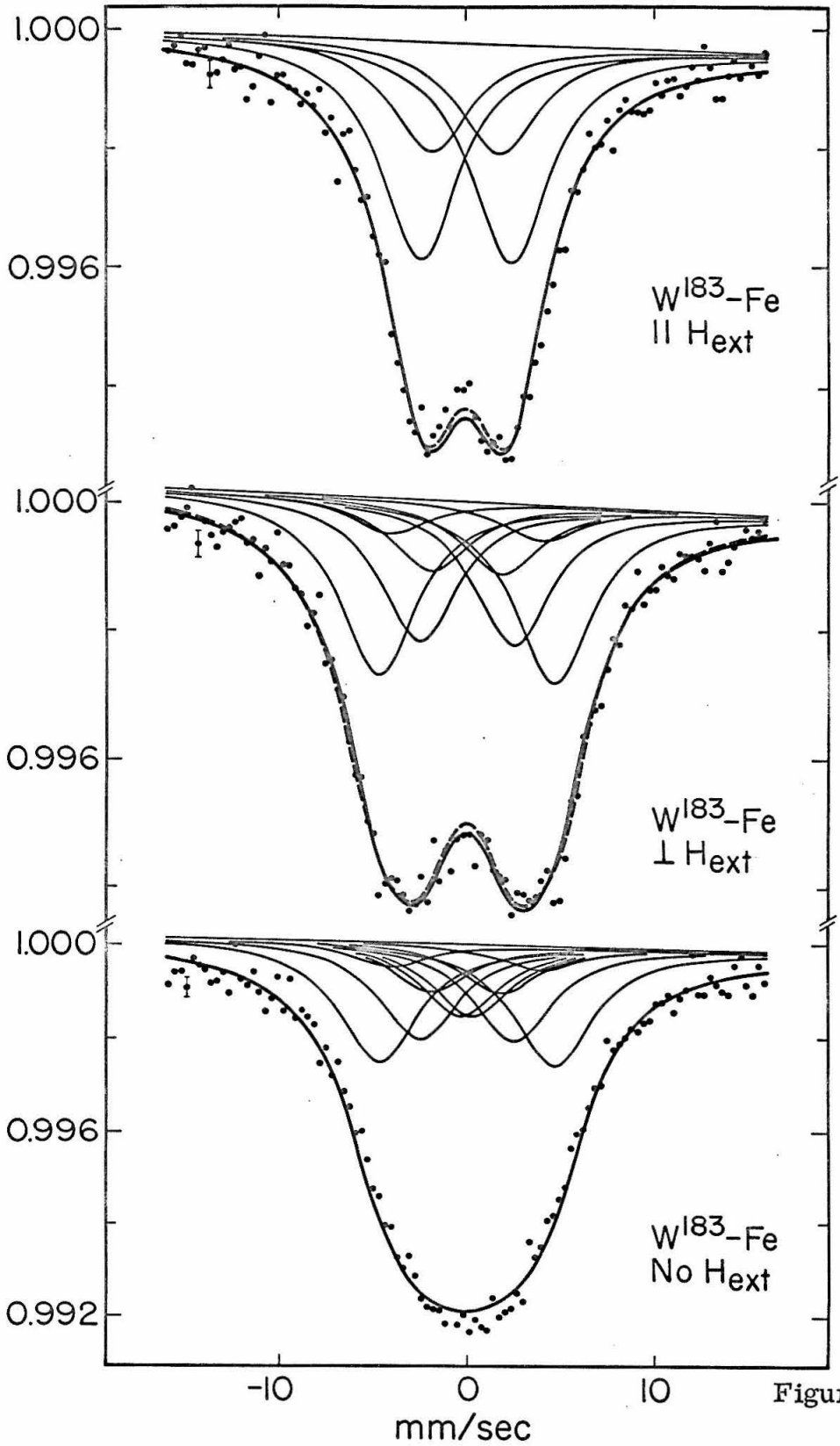
1.000
0.996
W183-Fe
II Hext
1.000
0.996
W183-Fe
⊥ Hext
1.000
0.996
W183-Fe
No Hext
0.992
-10
0
10
mm/sec

Figure III. 3

Figure III. 4

Velocity spectra for the Au^{195} source versus Pt-Fe absorbers for the different field configurations.

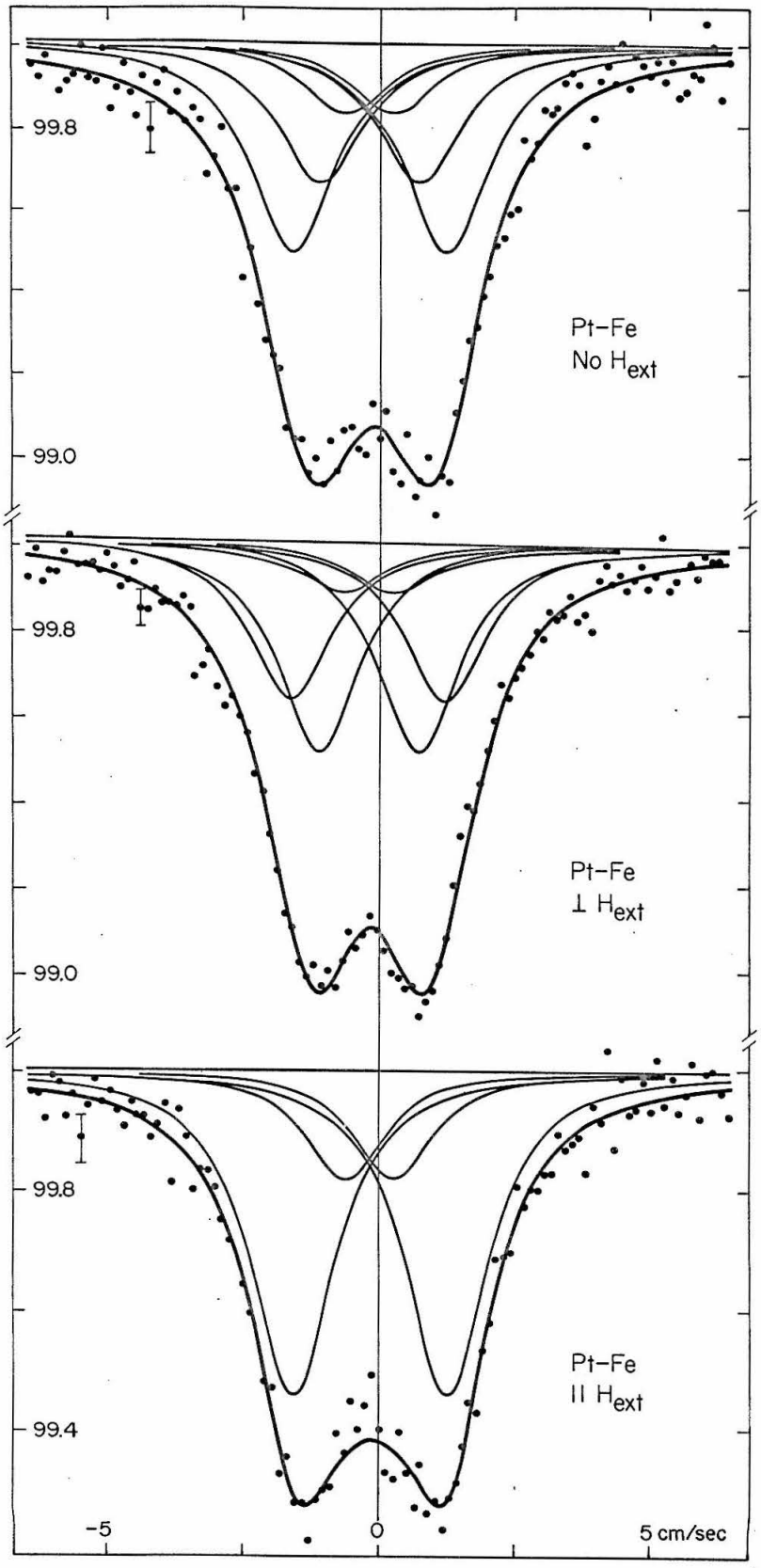
99.8
99.0
Pt-Fe
No H_{ext}
99.8
99.0
Pt-Fe
⊥ H_{ext}
99.8
99.4
Pt-Fe
II H_{ext}
-5
0
5 cm/sec

Figure III.4

Figure III. 5

Velocity spectra for the Au^{195} source versus absorbers of Pt-Co, Pt-Ni, and Pt.

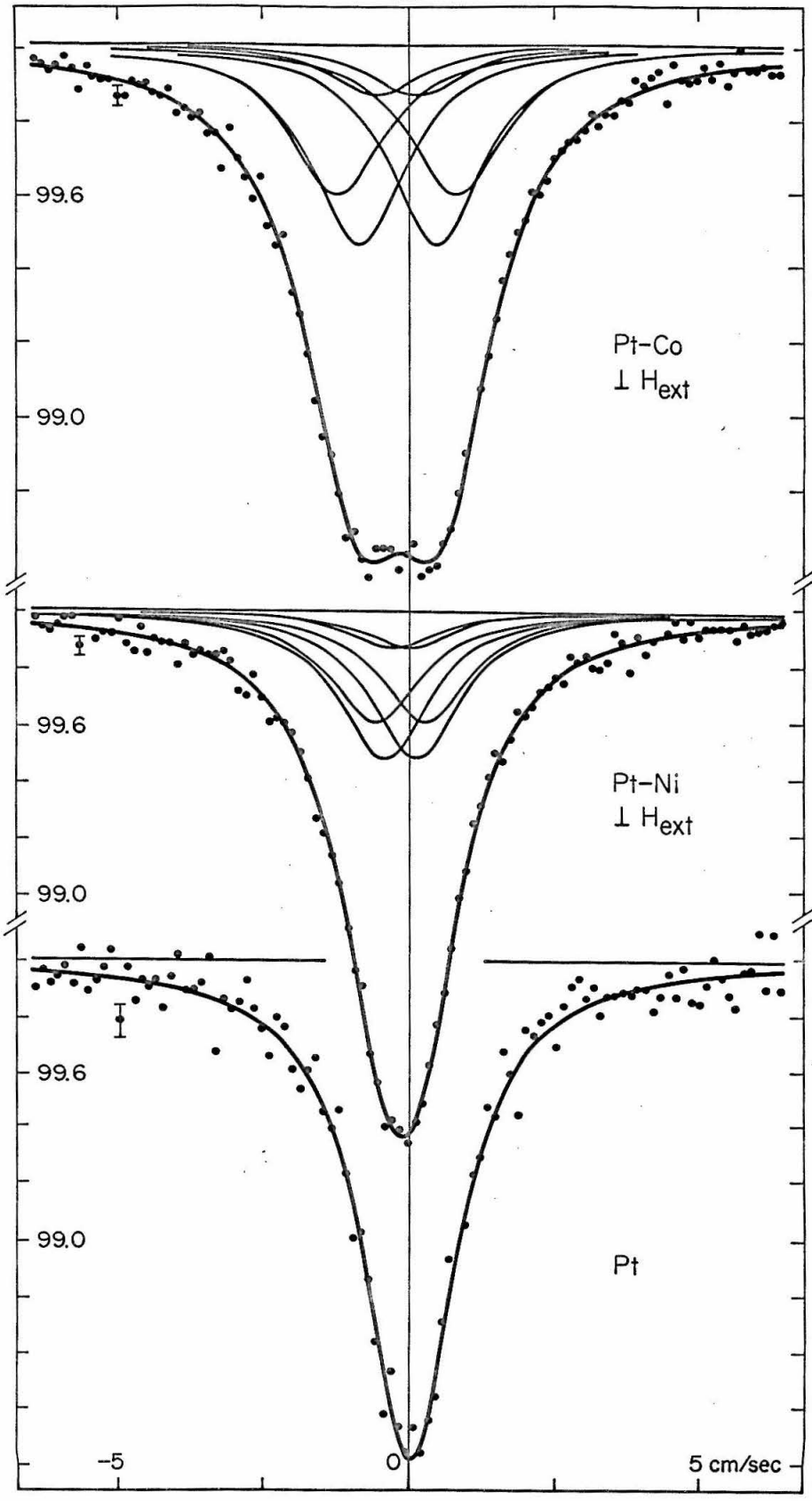

Figure III.5

Figure III.6

Plot of the isomeric shift of platinum alloys versus the electronegativity of the host element. The deviation for Pt-Al from the general trend might be because the platinum is not in a solid solution. In the insert isomeric shifts for some platinum compounds are shown related to the valency of platinum.

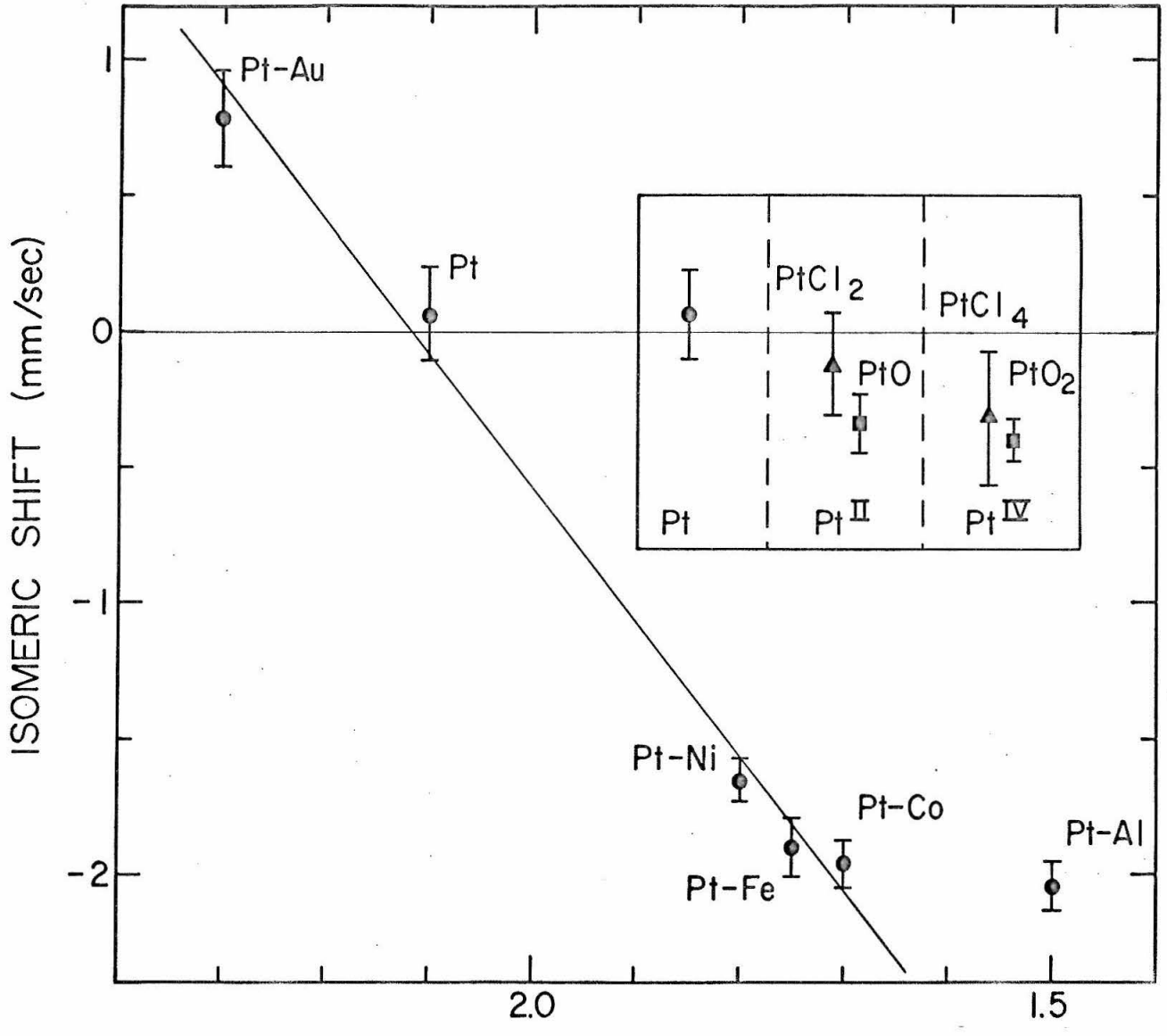
ISOMERIC SHIFT (mm/sec)
1
0
-1
-2
Pt-Au
Pt
Pt-Ni
Pt-Co
Pt-Fe
Pt-Al
PtCl2
PtCl4
PtO
PtO2
Pt
Pt II
Pt IV
2.0
1.5
ELECTRONEGATIVITY

Figure III.6

Figure III.7

Electric quadrupole patterns observed for the $0^+ - 2^+$ transition in W^{182} for absorbers of laboratory prepared tungsten disulfide and tungstic oxide. For WS_2, the solid curves correspond to the fit obtained with peak intensities fixed to the ratio 2:2:1, and the dashed curves are obtained with independently variable peak intensities. For WO_3, the solid curves correspond to the fit with variable symmetry parameter η; the dashed curves are obtained with $\eta = 0$.

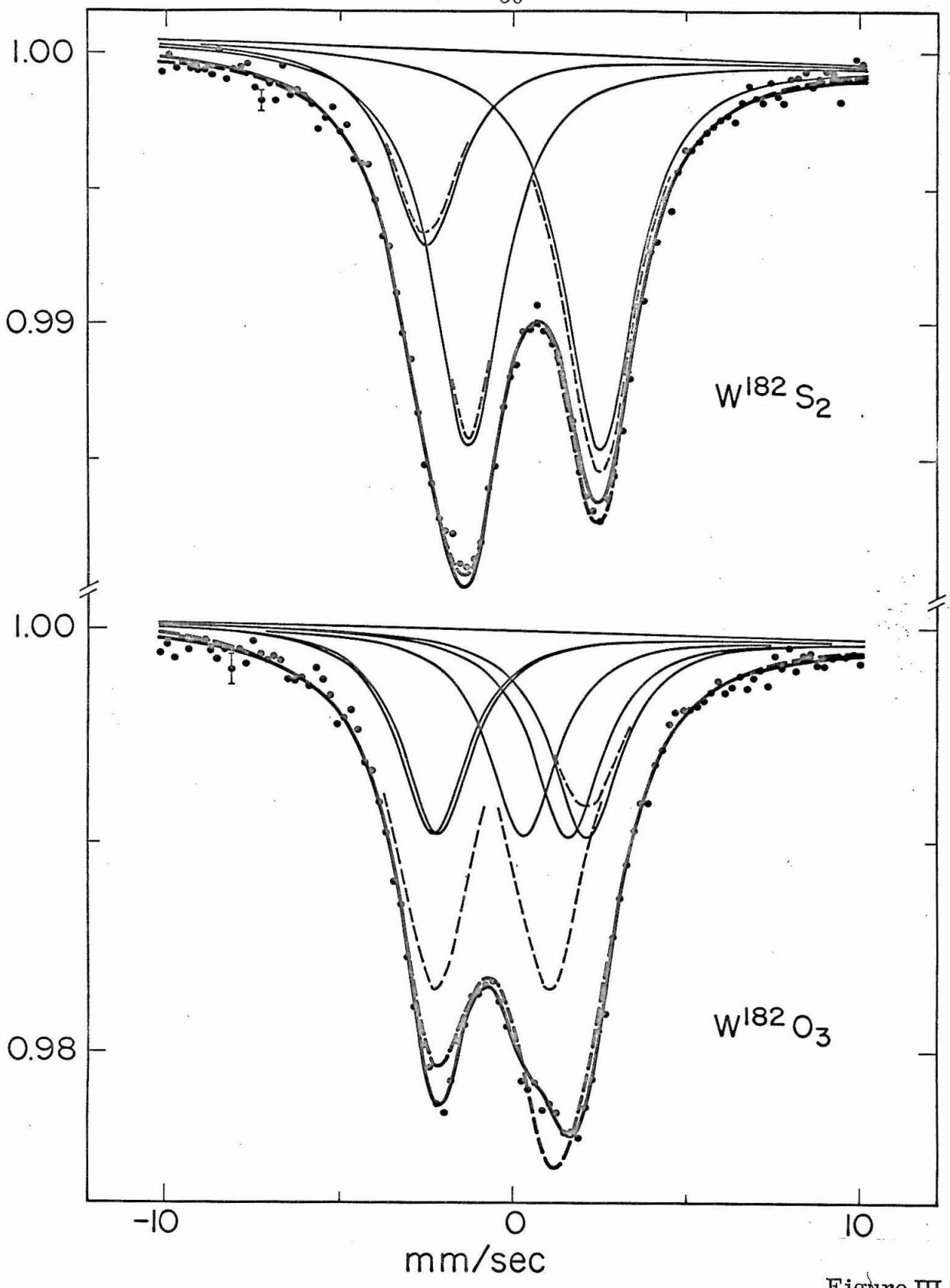

Figure III.7

Figure III. 8

Electric quadrupole patterns observed for the $0^+ - 2^+$ transition in W^{182} for absorbers of commercially obtained WS_2 taken at nitrogen and helium temperatures. The solid curves correspond to the fits obtained with peak intensities fixed to the ratio 2:2:1, and the dashed curves are obtained with independently variable peak intensities.

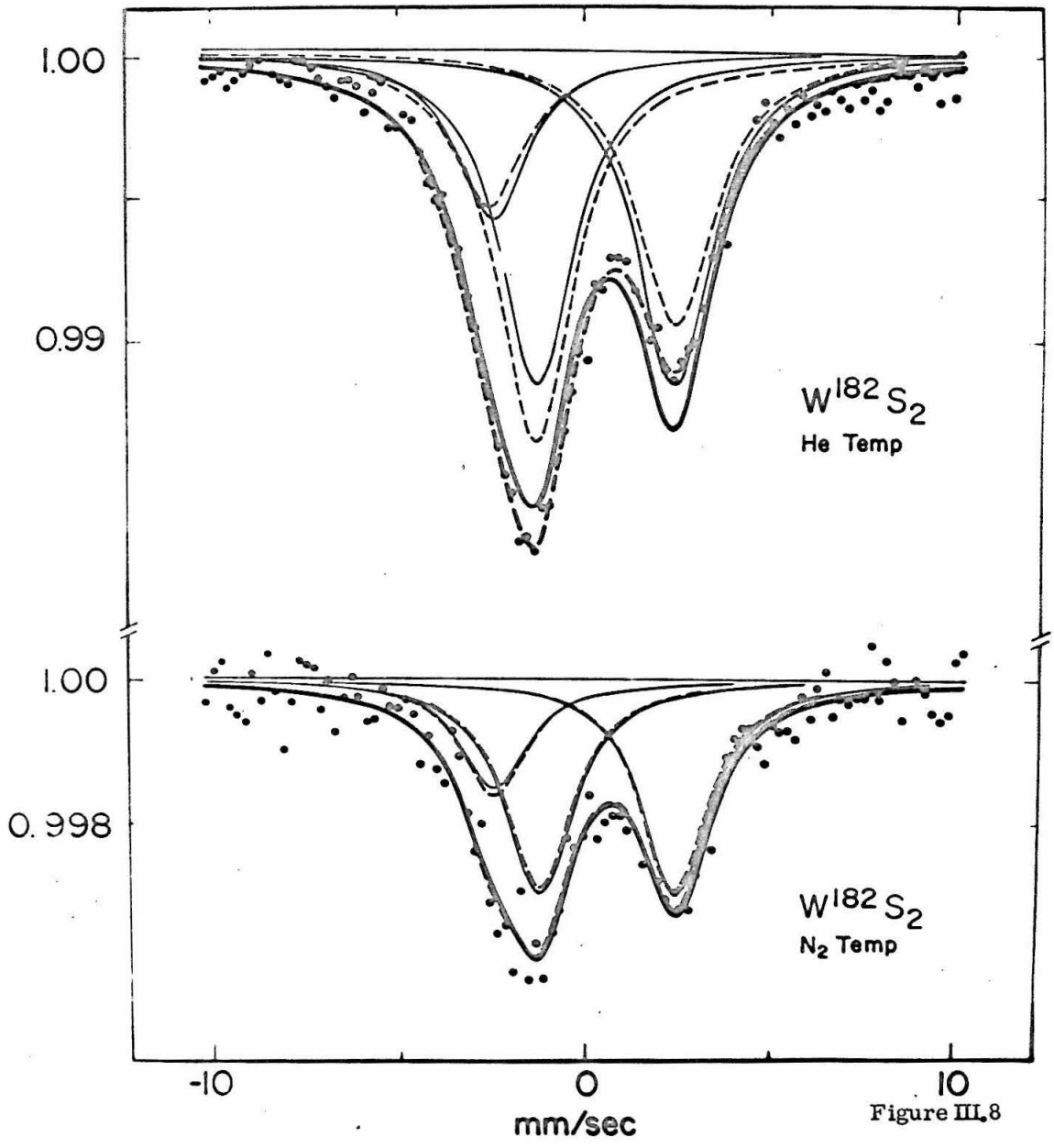

Figure III.8

Figure III. 9

Electric quadrupole patterns observed for the $1/2^- - 5/2^-$ transition in W^{183} for absorbers of enriched tungsten disulfide and tungstic oxide. Solid and dashed curves correspond to those in Figure 5. The lower spectrum is obtained with an absorber of enriched tungsten metal powder.

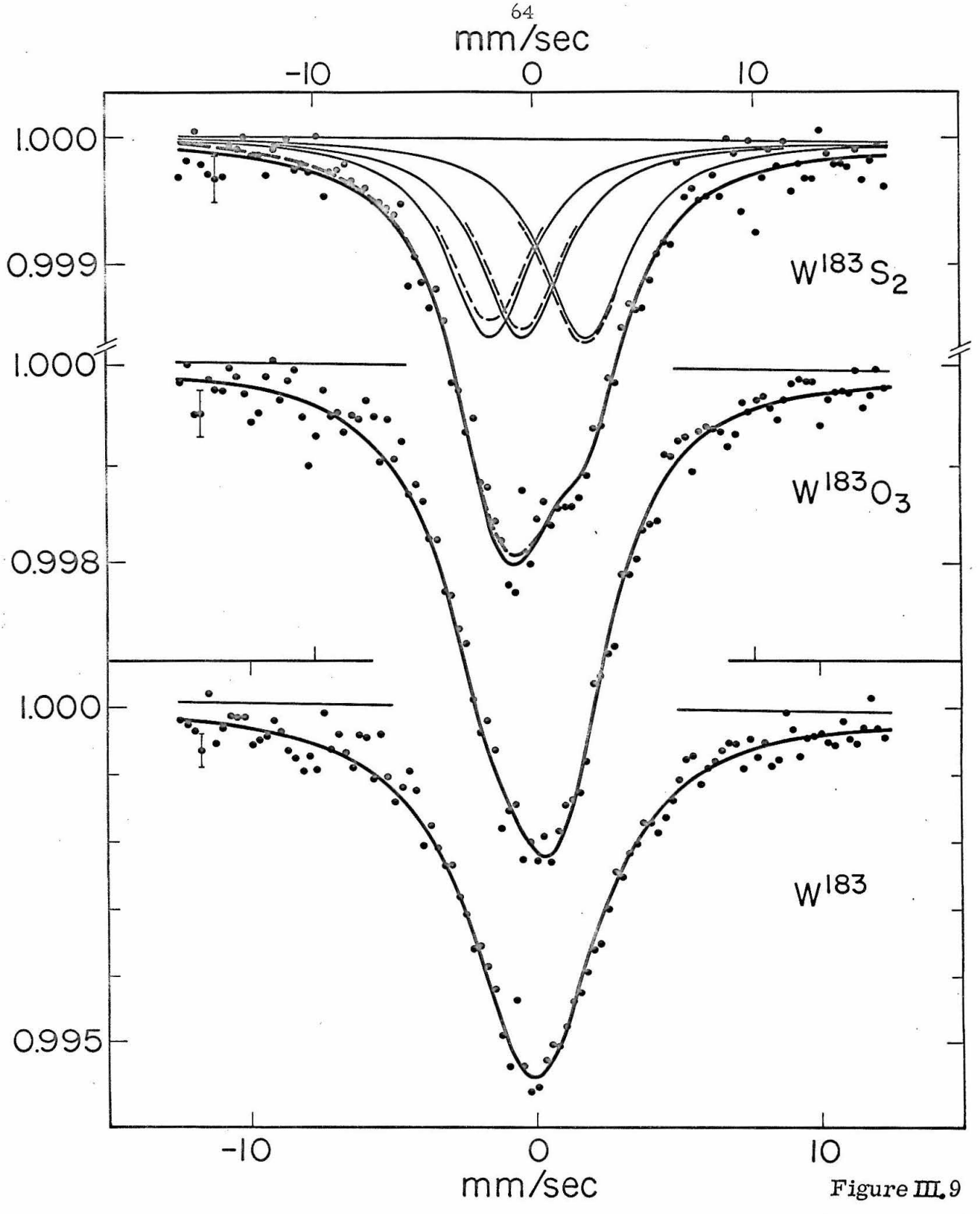
mm/sec
-10
0
10
1.000
0.999
1.000
0.998
1.000
0.995
W183S2
W183O3
W183
-10
0
10
mm/sec

Figure III.9

Figure III. 10

The dependence of the measured width on the absorber thickness for the $(3/2^- - 1/2^-)$ 47-keV transition in W^{183} and absorbers of W, W-Ni, and W-Fe. Note the shifted scales for the widths. An experimental point indicates the width of the Lorentzian fitted to the measured velocity spectrum, and the error-bars correspond to standard deviations. One measurement for W-Ni corresponding to the point (15.3; 55.9 ± 2.4) is not shown in the diagram; the point falls exactly on the extension of the solid line. A solid line corresponds to the thickness dependence of the width of one single Lorentzian, determined by the combined fitting of all the measured velocity spectra for the particular absorber material. The error bars on the vertical axis give the standard deviation of the extrapolated width determined from the combined fit. For W the dashed lines give the width dependence expected for solid tungsten absorbers. They were obtained by correcting the fitted solid line for granularity effects. The average grain size ($\approx 3.5\ \mu$) was measured and the following values were assumed for the Debye temperature (θ_D) and for the total internal conversion coefficient (α_t) : a) $\theta_D = 360^oK$, $\alpha_t = 7.6$, b) $\theta_D = 320^oK$, $\alpha_t = 8.4$, c) $\theta_D = 280^oK$, $\alpha_t = 9.2$. For W-Fe the dashed line gives the width of the composite spectrum at half maximum determined by the fit.

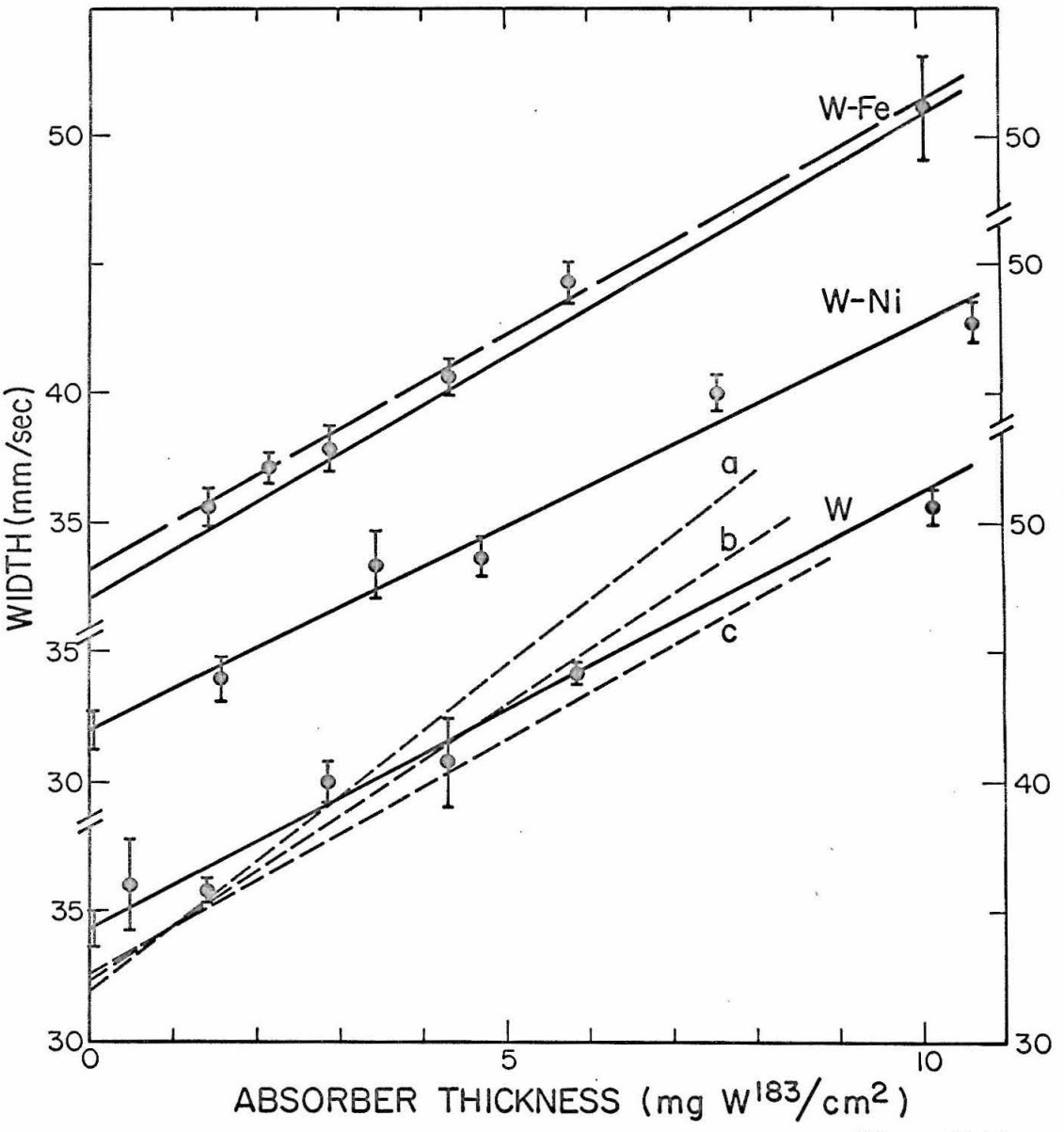

Figure III.1C

Table III.1

Transitions between magnetic substates and relative transition intensities. The transition intensities are based on Equation I.12 of Section I.20, where the symbols are explained, and are given for each field configuration used.

Table III.1

Transitions Between Magnetic Sublevels and Relative Transition Intensities

Nucleus												
W^{183}:	I'	5/2	m'	5/2	3/2	1/2	-1/2	-3/2	3/2	1/2	-1/2	-3/2	-5/2
	I	1/2	m	1/2	1/2	1/2	1/2	1/2	-1/2	-1/2	-1/2	-1/2	-1/2
	L	2	Δm	2	1	0	-1	-2	2	1	0	-1	-2
Intensity			No H_{ext}	5	4	3	2	1	1	2	3	4	5
			$\parallel H_{ext}$	0	4	0	2	0	0	2	0	4	0
			$\perp H_{ext}$	5	4	0	2	1	1	2	0	4	5
Pt^{195}:	I'	3/2	m'	3/2	1/2	-1/2	1/2	-1/2	-3/2				
	I	1/2	m	1/2	1/2	1/2	-1/2	-1/2	-1/2				
	L	1	Δm	1	0	-1	1	0	-1				
Intensity			No H_{ext}	3	2	1	1	2	3				
			$\parallel H_{ext}$	3	0	1	1	0	3				
			$\perp H_{ext}$	3	4	1	1	4	3				
W^{182}:	I'	2	m'	2	1	0	-1	-2					
	I	0	m	0	0	0	0	0					
	L	2	Δm	2	1	0	-1	-2					
Intensity			No H_{ext}	1	1	1	1	1					
			$\parallel H_{ext}$	0	1	0	1	0					
			$\perp H_{ext}$	1	1	0	1	1					

Table III. 2

Results from the study of the magnetic hyperfine interactions. Numbers within parentheses are standard deviations. The errors given are standard deviations increased to include the spread of the values and to take account of the uncertainties in the corrections as well as the precision of the velocity calibration. H_{int} corresponds to H_{eff} of the text.

Table III. 2

Source	Absorber	Thickness mgW/cm^2	Fitted Width mm/sec	Corrected Width mm/sec	Excited State Splitting mm/sec	$\lvert H_{int} \rvert$ [h] kG	$\lvert H_{int} \rvert / \mu_{eff}$ [h,j] kG/magneton	Comments [a]	$\frac{\chi^2}{N-n}$
Ta^{182}	W-Fe	44	2.40 (0.04)	2.28	1.596 (0.008)	715 ± 10	320	CF 0,⊥,∥	1.08 (0.05)
	W-Fe [b]	32	2.45 (0.04)	2.36	1.519 (0.009)	680 ± 10		CF 0,⊥,∥	0.95 (0.04)
	W-Co	33	2.43 (0.11)	2.34	0.806 (0.015)	360 ± 10	190	SF ⊥	1.19 (0.14)
	W-Ni	24	2.30 (0.11)	2.24	0.200 (0.043)	90 ± 25	150	SF ⊥	1.43 (0.14)
	W	20	2.52 (0.06)	2.23 2.30±0.06 [c]				SLF	0.95 (0.14)
					Ground State Splitting		$g(5/2^-)$ [h,k]		
Ta^{183}	W*-Fe	48	4.90 [d] (0.20)	4.55	0.89 (0.48)	400 (220)	0.53 (0.26)	CF 0,⊥,∥ [e]	1.19 (0.05)
	W*-Fe	48	5.08 [d] (0.12)	4.73	1.57 g)		0.327 (0.002)	CF 0,⊥,∥	1.19 (0.05)
	W*-Fe	48	5.12 [d] (0.12)	4.77	1.57 g)		0.338 (0.002)	CF ⊥,∥	0.92 (0.07)
	W*-Fe	48	4.62 [d] (0.15)	4.30	1.57 g)		-0.237 (0.003)	CF 0,⊥,∥ [f]	1.47 (0.05)
	W*	22	5.35 (0.18)	4.67 4.7 ± 0.2 [c]			0.34 ± 0.01 [c]	SLF	0.94 (0.14)

a) CF - Combined fit; SF - fit to a single velocity spectrum; SLF - fit to a single Lorentzian-shaped curve; 0 - No applied field; ⊥ - transverse applied field; ∥ - longitudinal applied field.
b) Alloy prepared by arc melting.
c) The value is an average of the appropriate separate determinations.
d) The quoted value corresponds to the spectra for the transverse field configuration.
e) Attempted determination of both the internal field and the g-factor.
f) Attempted determination of a negative value for the g-factor.
g) Determined from the results for W^{182}.
h) The given values correspond to adopting $g(2^+) = 0.24$, see text.
j) μ_{eff} taken from Ref. 25.
k) $g(5/2^-)$ is independent of the value of the width of the component Lorentzians. Fixing this width to values differing by as much as 30% does not affect $g(5/2^-)$.
*) Enriched tungsten was used for the absorber

Table III. 3

Results from the study of the 99-keV level in Pt^{195}. The errors given are standard deviations. H_{int} corresponds to H_{eff} of the text. The widths (W) are extrapolated to zero absorber thickness using $\theta_D(Pt) = 230^{o}K$ and the relation $\theta_D = \theta_D(host) \cdot \sqrt{M(host)/M(impurity)}$.

Table III.3

	Pt-Fe	Pt-Co	Pt-Ni	Pt
Thickness (mg Pt/cm^2)	30-60	50	50	50
$g_{3/2}$	-0.41 ±0.03	-0.41 *	-0.41*	
H_{int} (MG)	1.19 ±0.04	0.86 ±0.03	0.36 ±0.04	
W (mm/sec)	17.4 ±0.3	18.6 ±0.4	17.8 ±0.6	18.0 ±0.4
I.S. (mm/sec)	-1.90 ±0.11	-1.96 ±0.09	-1.65 ±0.08	0.06 ±0.17
H_{int}/μ_{eff} (MG/magneton)	0.54 ±0.02	0.46 ±0.02	0.58 ±0.06	

* Value adopted from the Pt-Fe results.

Table III. 4

Electric quadrupole hyperfine interaction for the $(2^+ - 0^+)$ transition in W^{182} and the $(5/2^- - 1/2^-)$ transition in W^{183}. Equation (I. 16) has been solved for the energy E and the form of the substates ψ resulting from the splitting of states with I = 2 and I = 5/2. The relative transition intensities T between these substates and the unsplit ground state are given as derived from Equation (I. 14). The quantity e^2qQ is the electric quadrupole splitting factor.

Table III. 4

$\eta = 0$ (as for WS_2)

I = 2			I = 5/2		
E	ψ	T	E	ψ	T
$-(1/4)e^2qQ$	$\|0\rangle$	1	$-(1/5)e^2qQ$	$\|\pm 1/2\rangle$	1
$-(1/8)e^2qQ$	$\|\pm 1\rangle$	2	$-(1/20)e^2qQ$	$\|\pm 3/2\rangle$	1
$+(1/4)e^2qQ$	$\|\pm 2\rangle$	2	$+(1/4)e^2qQ$	$\|\pm 5/2\rangle$	1

$\eta \neq 0$ (as for WO_3)

I = 2

E	ψ	T
$-(1/4)e^2qQ(1 + \eta^2/3)^{1/2}$	$\|+2\rangle + \|-2\rangle$ $-(\sqrt{6}/\eta)[1+(1+\eta^2/3)^{1/2}]\|0\rangle$	1
$-(1/8)e^2qQ(1 + \eta)$	$\|+1\rangle - \|-1\rangle$	1
$-(1/8)e^2qQ(1 - \eta)$	$\|+1\rangle + \|-1\rangle$	1
$+(1/4)e^2qQ$	$\|+2\rangle + \|-2\rangle$	1
$+(1/4)e^2qQ(1 + \eta^2/3)^{1/2}$	$\|+2\rangle + \|-2\rangle$ $-(\sqrt{6}/\eta)[1-(1+\eta^2/3)^{1/2}]\|0\rangle$	1

I = 5/2

$E_j = (1/40)e^2qQ \cdot$ (jth solution of the equation:

$$x^3 - 28x(3 + \eta^2) - 160(1 - \eta^2) = 0)$$

$\psi_j = a_j|\pm 5/2\rangle + b_j|\pm 1/2\rangle + c_j|\mp 3/2\rangle$

$T_j = 1,\ j = 1,\ 3$

Table III.5

Results from the study of quadrupole interactions. Numbers within parentheses are standard deviations.

Table III.5

Source	Absorber[a]	Fitted Width[b] mm/sec	$\frac{ce^2qQ}{E_\gamma}$ mm/sec	Electric Field Gradient e) eq 10^{18} V/cm^2	$\frac{Q(5/2^-)}{Q(2^+)}$	Relative Peak Intensities or Asymmetry Parameter	$\frac{\chi^2}{N-n}$
Ta^{182}	WS_2	2.49 (0.04)	10.04 (0.06)			2:2:1 d)	1.58
		2.50 (0.04)	10.07 (0.06)	-1.86 ± 0.05		2.12:1.96:0.93	1.01
	WO_3	2.84 (0.08	-8.73 (0.09)			2:2:1 d)	8.18
		2.76 (0.06)	-8.23 (0.10)			2.12:1.41:1.47	4.25
		2.42 (0.04)	-8.34 (0.05)	+1.54 ± 0.04		η = 0.63 ± 0.02	2.18
Ta^{183}	W^*S_2	4.8 (0.3)	9.45 (0.40)		0.931 ± 0.038	1:1:1 d)	0.93
		4.7 (0.3)	9.55 (0.38)		0.939 ± 0.036	1.06:0.99:0.95 d)	0.92
	W^*O_3	5.1 (0.3)	-7.92 (0.37)		0.940 ± 0.050	η = 0.63 d)	1.10
	$Q(5/2^-)$ = - (1.70) ± 0.07) barns e)						

a) The thicknesses were 50 mgW/cm^2 and 22 mgW*/cm^2, where the symbol * stands for enriched material.
b) Not corrected for absorber thickness.
c) The standard deviation of $\chi^2/(N-n) \approx 0.14$ for all the fits.
d) Kept fixed in the fitting procedure.
e) Adopting $Q(2^+)$ = - (1.81 ± 0.05) barns, inferred from Coulomb excitation experiments (Ref. 30).

IV. DISCUSSION

IV. DISCUSSION

1) Magnetic Fields

The internal magnetic field (715 ± 10 kG; see Table III. 2) at tungsten nuclei in dilute solution in iron determined in the present work is in agreement with that (700 ± 70 kG) obtained in an earlier Mössbauer experiment[21] and the NMR result (635 kG) of Kontani and Itoh,[22] but is inconsistent with the value (430 ± 100 kG) determined by the Coulomb-excitation technique.[23] There is better agreement among the results of the present measurements of the internal fields for tungsten in cobalt (360 ± 10 kG) and nickel (90 ± 25 kG) and the fields obtained in Coulomb-excitation experiments[23] (Co: 330 kG; Ni: 60 kG). The NMR result for W in Co is 385 kG.[22]

The discrepancy between the values of the internal field in W-Fe obtained by Mössbauer and NMR experiments and the value obtained by the Coulomb-excitation technique is not at all understood. The discrepancy might be due to a dependence of the field on the concentration, since vastly different concentrations were used in the Mössbauer and the NMR experiments as compared to the Coulomb-excitation experiments. However, for concentrations from 0.18 to 3.6 at. % tungsten we found no such dependence for tungsten-iron alloys. Herskind et al.[24] have found a similar discrepancy for Pd-Fe alloys, and they contend that the implantation technique used in the Coulomb-excitation experiments results in a different internal field from that obtained with a metallurgically prepared alloy. This may be because the nucleus recoilling into the lattice produces local disturbances which are not present in the metallurgically prepared sample. Finally there may be a temperature dependence of the internal field, since both the Mössbauer and the NMR experiments

were done at liquid helium temperature, while the Coulomb excitation was done at room temperature.

The internal field (1190 ± 40 kG; see Table III.3) for Pt in Fe obtained in the present work is in rough agreement with the NMR result[22] (1280 kG). There is better agreement between our results for Pt-Co (860 ± 30 kG) and Pt-Ni (360 ± 40 kG) and the NMR results (830 and 340 kG, resp.).

Figure IV.1 shows the variation of the internal field H_{eff} for several elements in dilute solid solution in Fe, Co, and Ni as a function of the magnetic moment μ_{eff} (μ_{host}) on the host atom. Shirley and Westenbarger[25] have attempted to explain the internal fields of transition elements dissolved in magnetic hosts of the 3d transition series. Their approach assumes that the major portion of the field is due to a polarization of conduction electrons (CEP) by an exchange interaction involving the conduction electrons and the 3d electrons of the host atom. Their explanation predicts a linear dependence of the internal field on the host magnetic moment. As is seen in Figure IV.1, the fields for tungsten and to a lesser extent platinum, deviate from this predicted linear dependence. Their explanation is therefore incomplete.

Although Shirley and Westenbarger mention other mechanisms that could possibly contribute to the internal field, they do not consider these to be important. However, the trend of our data for tungsten and platinum indicate that their premise is not valid. When an impurity element of a transition series is dissolved in a magnetic host of the 3d transition series, the spin of the host polarizes the spin of the d shell of the impurity, which in turn polarizes the core electrons. After Campbell[26], the polarization of the core (CP), and the field produced by CP, is taken to be

proportional to the magnetic moment of the impurity, $\mu_{impurity}$. Thus, for W and Pt, elements of the 5d transition series, both CEP and CP contribute to H_{eff}, which may therefore be written as

$$H_{eff} = a\ \mu_{impurity} + b\ \mu_{host}\ . \qquad (IV.1)$$

The parameter a, which gives the contribution to the internal field from CP, is not expected to vary with the number of d electrons within a given transition series, because the core electrons are predominately inside the d shell.[27] By contrast the contribution to the field from CEP, given by the parameter b, varies markedly within a given series,[25] since the d electrons vary from element to element and provide variable shielding for the conduction electrons. Values for $\mu_{impurity}$ for a number of transition elements, including W and Pt, in Fe have been derived by Campbell[26] from neutron diffraction data. For Fe, Co, and Ni, $\mu_{host} \approx$ 2.22, 1.72, and 0.606 Bohr magnetons, resp.[28),29]

Our confidence in the validity of Equation IV.1 is increased by considering the data presented in Figure IV.1 for Au, Ag, and Cu. These elements are diamagnetic atoms at the end of each of the transition series. Since they have no magnetic moments, there is no contribution from CP. The internal field is then given by the second term alone of Equation IV.1, in agreement with the linear dependence evident from the figure. It is thus reasonable to assume that the deviation from the linearity that was predicted by Shirley and Westenbarger is due to the additional contribution to the field from CP.

2) Nuclear Parameters for the $5/2^-$ and $3/2^-$ States in W^{183}

This experiment provides the first measurement of the electric quadrupole moments of the $5/2^-$ (99-keV) state in W^{183} and of the magnetic moments of the $5/2^-$ and $3/2^-$ (46.5-keV) states. A value for the lifetime of the $5/2^-$ state is estimated in this work, but large corrections had to be made which were based on assumptions that are not well established (see Section III.4b). A reliable measurement is made of the lifetime of the $3/2^-$ state. Previous estimates for these lifetimes have been made based on Coulomb-excitation experiments[30] and the Mössbauer experiment of Sumbaev et al.[31] However, the present result for the $3/2^-$ lifetime represents a considerable improvement over the previous values.

The nuclide W^{183} is a strongly deformed nucleus whose level scheme consists of several bands (see Figure I.1). The level structure and the γ-ray transition intensities in this nucleus cannot be well accounted for by an adiabatic rotational model for the nucleus. A significantly improved description was obtained by Kerman[32] as the result of mixing of states in the two low-lying bands, $K = 1/2$ and $3/2$, by Coriolis coupling (the RPC model). More extensive band mixing has been considered by Rowe[33] and by Brockmeier et al.[34] In this section a comparison of the experimental results with calculations in terms of the RPC model will be made. The results of the work of Brockmeier et al., namely the mixing parameters and magnetic matrix elements, and its notation will be used. The admixture of states of the higher bands into the low-lying levels is very small. Therefore mixing of states in only the two lower bands is considered. Thus the moments and the M1 and E2 transition probabilities can be described by the following eight matrix elements:[34]

$G^{1/2\ 1/2}$, $G^{1/2\ 1/2}b_{M1}$, $G^{1/2\ 3/2}$, $G^{3/2\ 3/2}$, and $Q^{1/2\ 1/2}$, $Q^{1/2\ 3/2}$, $Q^{1/2\ 3/2}b_{E2}$, $Q^{3/2\ 3/2}$, where $G^{KK} = K(g_K - g_R)$ and $b_{M1} = b_0\sqrt{2}$.

The accurately determined ratio of the quadrupole moments, $Q(5/2^-)/Q(2^+) = 0.94 \pm 0.04$ (see Table III. 5), suggests a comparison with accurately measured B(E2) values for Coulomb excitation in W^{182} and W^{183}.[30] The comparison is presented in Figure IV. 2. In this figure $Q(5/2^-)$ may have been incorrectly derived. Our determination of its value depended on the derivation of $Q(2^+)$ from $B(E2;\ 0^+ \rightarrow 2^+)$. In this derivation we assumed the correctness of the rotational model for W^{182}. However, recent Mössbauer experiments[35] in W^{186} and the theoretical calculations of Kumar and Baranger[36] have cast doubt on this assumption. Thus, the inconsistency apparent from the graph may be due to an incorrect value for $Q(5/2^-)$. In any case the diagram allows the determination of $Q^{1/2\ 1/2} = 6.5 \pm 0.3$b and $Q^{1/2\ 3/2}b_{E2} = -0.4 \pm 0.5$b.

The measured magnetic moments, $\mu(3/2^-)$ and $\mu(5/2^-)$, and the measured half-life of the $3/2^-$ state can be compared with values derived from the magnetic parameters of Brockmeier et al. The latter were obtained from the fit to a large number of relative γ-ray transition intensities[37] with the assumption $Q^{1/2\ 1/2} = 6.5$b, which agrees with the value determined above. To calculate the magnetic moments the g-factor for the core rotation, g_R, must be assumed and is here taken equal to the g-factor of the ground state rotational band of W^{182}, since the contribution to g_R from the odd neutron has been accounted for in the band-mixing theory. Contributions to g_R due to higher bands and blocking effects are small compared to the uncertainty in the g-factor of W^{182}. The comparison

is presented in Table IV. 1. It is seen that $\mu(1/2^-)$ is well accounted for, but $\mu(3/2^-)$, $\mu(5/2^-)$, and B(M1; $3/2^- - 1/2^-$) differ from the predictions of Brockmeier et al.

Recently, new experimental information on the W^{183} nucleus has become available,[38),39)] which, together with the results of the present experiment, calls for a redetermination of the magnetic single-particle matrix elements. The data used are the results of the present measurements, the value of the ground state magnetic moment, and those B(M1) values for transitions of predominantly magnetic character that can be determined most precisely. In Table IV. 1 are listed the experimental quantities used. These are fitted to the theoretical magnetic transition rates and moments[32),34)] with the least-squares method. The fit is found to be insensitive to the parameters $G^{1/2\ 3/2}$ and $G^{3/2\ 3/2}$. The influence of various constraints on these parameters was investigated to determine the reliability of the values obtained for the parameters g_R, $G^{1/2\ 1/2}$, and $G^{1/2\ 1/2}b_{M1}$. The results of such a fit are also included in the table. It was also found that these latter parameters do not depend sensitively on any individual experimental quantity. The following values are the results of the fits:

$$g_R = 0.25 \pm 0.04$$

$$G^{1/2\ 1/2} = -1.06 \pm 0.05$$

$$G^{1/2\ 1/2}b_{M1} = -0.74 \pm 0.06\ .$$

The Nilsson model allows us to understand the values of $G^{1/2\ 1/2}$ and $G^{1/2\ 1/2}b_{M1}$ by the expressions:

$$G^{1/2\ 1/2} \equiv (1/2)(g_K - g_R) = (g_\ell - g_R)\langle 1/2 \,|\, \hat{j}_z \,|\, 1/2 \rangle + (g_S^z - g_\ell)\langle 1/2 \,|\, \hat{s}_z \,|\, 1/2 \rangle \qquad \text{(IV. 2a)}$$

$$G^{1/2\ 1/2}b_{M1} \cdot \sqrt{2} \equiv (g_K - g_R)b_0 = (g_\ell - g_R')\langle 1/2 \,|\, \hat{j}_+ \,|\, -1/2 \rangle + (g_S^+ - g_\ell)\langle 1/2 \,|\, \hat{s}_+ \,|\, -1/2 \rangle \qquad \text{(IV. 2b)}$$

where, in the strict sense of the model, $g_S^z = g_S^+ = g_S$, the free nucleon value, and $g_R' = g_R$. The bras and kets refer to single-particle states. It is well known that the interaction between the spin of the odd nucleon and the spins of the nucleons in the core reduces the spin contribution to the nuclear magnetic moment, and that this effect can be accounted for by the use of an effective value in place of g_S. It has recently been pointed out by Bochnacki and Ogaza[41] that the component of the spin polarization of the core in the direction parallel to the symmetry axis of the nucleus might not be the same as that in a direction transverse to the symmetry axis. Therefore one may not assume that g_S^z and g_S^+ are equal. The term $(g_\ell - g_R')\langle 1/2 \,|\, \hat{j}_+ \,|\, -1/2 \rangle$ is only slightly affected by the spin polarization, so that $g_R' \approx g_R$,[41] and we have adopted $g_R = 0.24$, an average of several recent measurements.[8] The matrix element $\langle 1/2 \,|\, \hat{j}_+ \,|\, -1/2 \rangle$ can be obtained from the experimentally determined[34] decoupling parameter $a_0 = -\langle 1/2 \,|\, \hat{j}_+ \,|\, -1/2 \rangle$. Since the odd nucleon is a neutron, $g_\ell = 0$. Equations IV. 2 have been evaluated with various assumptions for the potential,[42),43)] and the effective single-particle g-factors, g_S^z and

g_S^+, are then obtained by comparison with the experimental values for $G^{1/2\ 1/2}$ and $G^{1/2\ 1/2}b_{M1}$. The effective single-particle g-factors are quoted in Table IV. 2.

For comparison, corresponding values for Yb^{171} and Tm^{169} have been calculated from available experimental data.[44-46] Since the primary experimental results have not been analyzed in terms of band mixing, one should in principle correct for the effects of band mixing on the experimental quantities g_K, g_R, and b_0.[47), 48] Such corrections have been estimated by assuming that only K = 3/2 bands mix with the K = 1/2 ground state.[47] One consequence of the neglect of the mixing of the K = 1/2 bands with the ground state is that no correction is obtained for the quantity $(g_K - g_R)b_0$. In Table IV. 2 are given the results of two calculations of the effective g-factors g_S^z and g_S^+, one accounting for Coriolis mixing with the K = 3/2 bands only and the other without Coriolis mixing.

It is demonstrated in the table that in all cases the values derived for g_S^z and g_S^+ using recent Nilsson wave functions[42] differ from each other significantly. It should be pointed out that the values calculated for the effective g-factors depend on the potential used in the nuclear model. If the old Nilsson wave-functions[43] are used, markedly changed values are obtained for the effective g-factors for Yb^{171}, viz. $g_S^z/g_S^+ < 1$, whereas there are only small changes for W^{183} and Tm^{169}.

3) Magnetic Moment for the $3/2^-$ Level of Pt^{195}

The value for the g-factor of the $3/2^-$ state determined in this experiment (-0.41 ± 0.03) is in good agreement with that of Atac et al.[49] (-0.43 ± 0.10) and with the recently quoted value

(-0.40 ± 0.07) of Buyrn and Grodzins.[50] It is just outside the limits $(0.47 > g_{3/2} > -0.60)$ given by Benczer-Koller et al.[51] who assume $|H_{int}| = 1.39$ MG for the Pt-Fe alloy. The core-excitation model proposed by de-Shalit[52] and Gal[53] should account for the low-energy states in Pt^{195}. Experimental information is available for the 2^+ states in Pt^{194} [54),55] so that a comparison of the predicted and measured values of the g-factor can be made. It turns out that calculations give values very near zero; hence present core-excitation models do not give an adequate description of the $3/2^-$ state in Pt^{195}. As has been pointed out,[53] the discrepancy might be removed if configuration mixing is taken into account.

Figure IV. 1

Internal fields H_{eff} at nuclei of atoms dissolved in Fe, Co, and Ni lattices, plotted against the host magnetic moment μ_{eff}. The values for W and Pt have been measured in this work. (See Tables III. 2 and III. 3.) The remaining values of H_{eff}, as well as the values of μ_{eff}, are taken from a similar figure in Shirley and Westenbarger (Ref. 25).

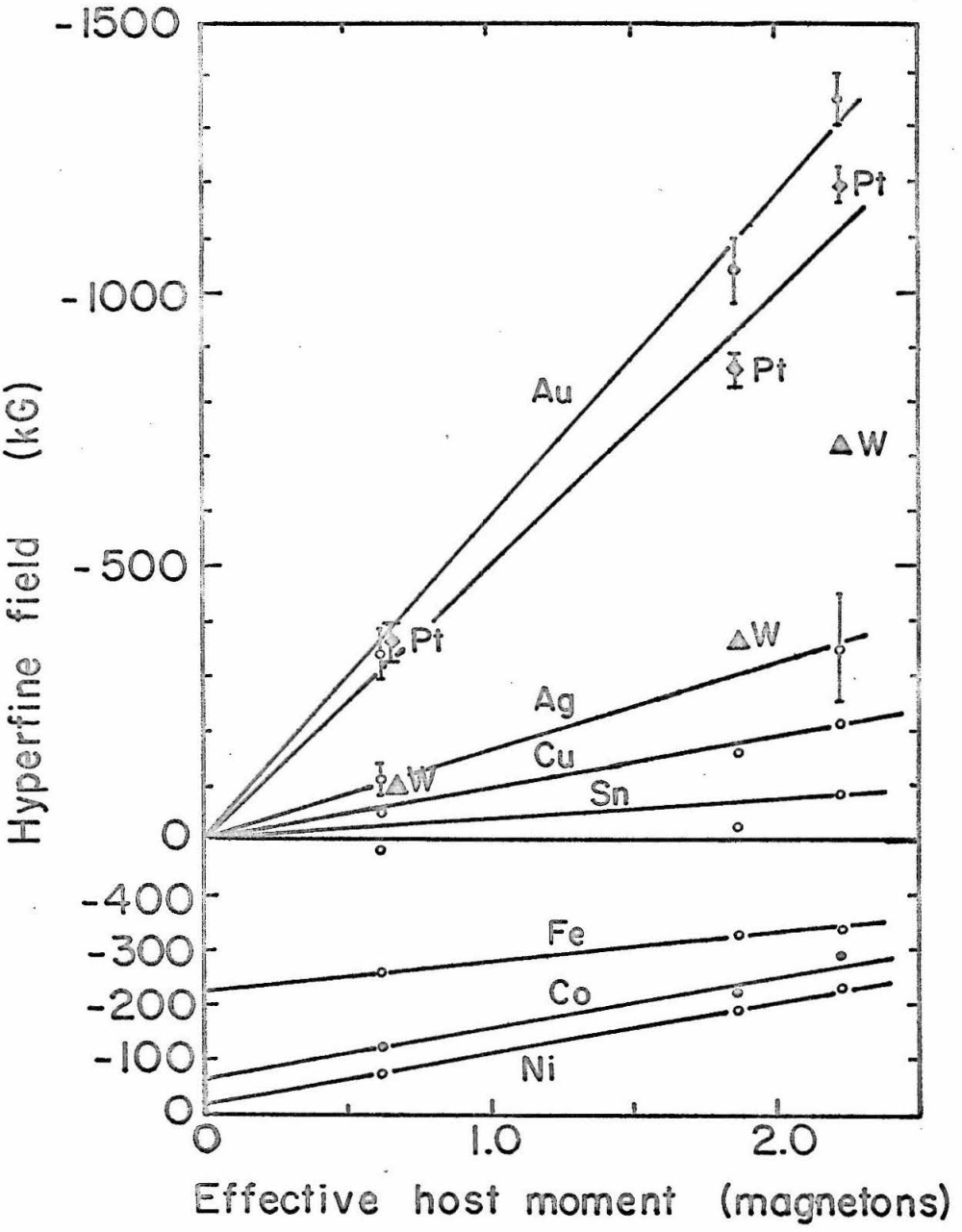
-1500
-1000
-500
0
-400
-300
-200
-100
0
Hyperfine field (kG)
Au
Pt
Pt
ΔW
Pt
ΔW
Ag
Cu
Sn
ΔW
Fe
Co
Ni
0
1.0
2.0
Effective host moment (magnetons)

Figure IV.1

Figure IV. 2

Comparison of the electric parameters for W^{183} derived from the ratio of the quadrupole moments, $Q(5/2^-)/Q(2^+)$, measured in the present experiment and B(E2) values measured by the Coulomb excitation technique (Reference 30). The ratio of the quadrupole moments and the $B(E2,\ 0^+ \rightarrow 2^+) = 4.00 \pm 0.20\ e^2b^2$ imply $Q(5/2^-) = 1.70 \pm 0.07$ b. The three quantities $Q(5/2^-)$, $[B(E2;\ 1/2^- \rightarrow 5/2^-)]^{1/2}$ depend linearly on the quantities $Q^{1/2\ 1/2}$, $Q^{1/2\ 3/2}$, $Q^{1/2\ 3/2}b_{E2}$, and $Q^{3/2\ 3/2}$. It is assumed that $Q^{1/2\ 3/2} = 0$; also $Q^{3/2\ 3/2}$ enters only in $Q(5/2^-)$ and is there of little importance.

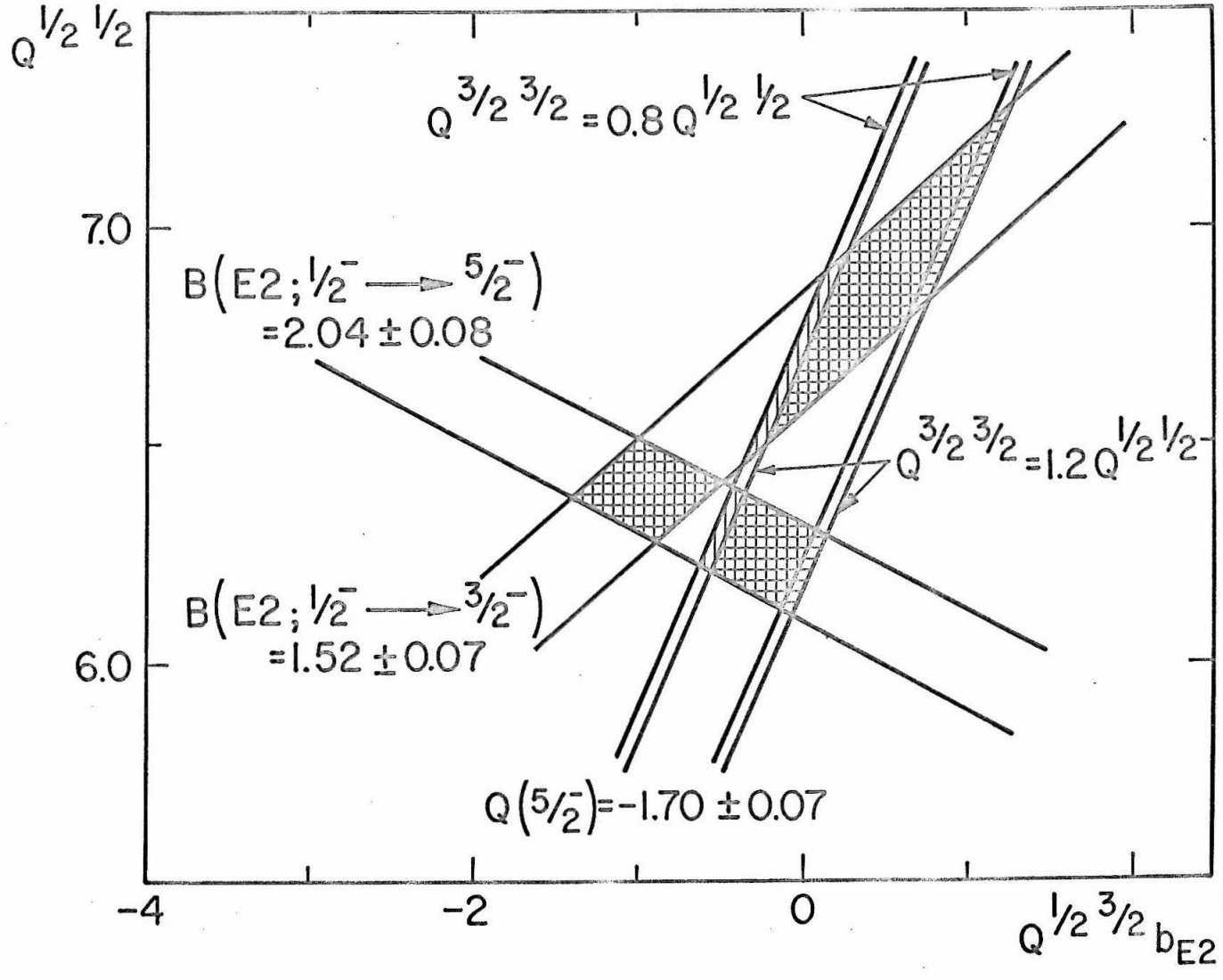
$Q^{1/2\ 1/2}$
7.0
6.0
$Q^{3/2\ 3/2} = 0.8\, Q^{1/2\ 1/2}$
$B(E2; 1/2^- \longrightarrow 5/2^-)$
$= 2.04 \pm 0.08$
$Q^{3/2\ 3/2} = 1.2\, Q^{1/2\ 1/2}$
$B(E2; 1/2^- \longrightarrow 3/2^-)$
$= 1.52 \pm 0.07$
$Q(5/2^-) = -1.70 \pm 0.07$
-4
-2
0
$Q^{1/2\ 3/2}\, b_{E2}$

Figure IV.2

Table IV. 1

Magnetic moments, B(M1) values, and magnetic parameters determined from these. The units for the magnetic moments and the B(M1) values are nm and $(nm)^2$, respectively. Column A gives the result of the fit with all parameters varied; column B corresponds to fixing the two parameters to which the fit is insensitive. Except where noted, the B(M1) values are determined from the following quantities:

1) The ratio of the γ-ray intensity of the appropriate transition to that of the crossover transition originating from the same level (averaged from those of References 37 and 38).

2) The B(E2) value for the crossover transition (calculated from the values of $Q^{1/2\ 1/2}$ and $Q^{1/2\ 1/2}b_{E2}$ given in the text); and

3) The mixing ratio for the direct transition (Reference 39).

Table IV.1

Quantity	Experimental Value	Predictions of Brockmeier et al.	Fits to Present Data	
			A b)	B
$\mu(1/2^-)$	0.117	0.123	0.117	0.117
$\mu(3/2^-)$	-0.1 ± 0.1	-0.28	-0.22	-0.08
$\mu(5/2^-)/\mu(2^+)$	1.75 ± 0.05	1.98	1.79	1.86
$B(M1, 3/2^- \rightarrow 1/2^-, 46.5)$ a)	0.209 ± 0.020	0.288	0.176	0.178
$B(M1, 5/2^- \rightarrow 3/2^-, 52.6)$	0.0239 ± 0.0017	0.0316	0.0256	0.0263
$B(M1, 7/2^- \rightarrow 5/2^-, 107.9)$	0.216 ± 0.029	0.245	0.193	0.164
$B(M1, 5/2^- \rightarrow 3/2^-, 82.9)$	$(0.94 \pm 0.26) \cdot 10^{-3}$	$1.39 \cdot 10^{-3}$	$0.98 \cdot 10^{-3}$	$1.02 \cdot 10^{-3}$
g_R		0.24 c)	0.25 (0.04)	0.28
$G^{1/2\ 1/2}$		-1.25	-1.06 (0.05)	-1.06
$G^{1/2\ 1/2}{}_{b_{M1}}$		-0.89	-0.74 (0.06)	-0.70
$G^{1/2\ 3/2}$		-0.21	-0.04 (0.13)	-0.21 d)
$G^{3/2\ 3/2}$		0.68	-0.2 (0.7)	0.68 d)

a) Calculated from $T_{1/2}(3/2^-)$ with $\alpha_t = 8.4$ (Ref. 40), and $\delta^2 = 0.006$ (Ref. 39).
b) Numbers within parentheses are standard deviations.
c) Adopted value, equal to g_R of the ground state rotational band in W^{182}; Brockmeier et al. use $g_R = 0.35$.
d) Fixed at the value predicted by Brockmeier et al. (Ref. 34).

Table IV. 2

Effective single-particle g-factors derived from the results of the present experiment (W^{183}) and from the experimental data of References 45, and 46 (Yb^{171}) and of Reference 44 (Tm^{169}). The matrix elements of the spin operators have been calculated from recent Nilsson wave functions (Reference 42), using the potential parameters $\kappa = 0.0637$ and $\mu = 0.42$. The errors quoted are derived from the uncertainties in the experimental data only.

Table IV. 2

Quantity	W^{183}	Yb^{171}	Tm^{169}
$\langle 1/2 \lvert s_z \rvert 1/2 \rangle$	0.281	-0.183	-0.356
$\langle 1/2 \lvert s_+ \rvert -1/2 \rangle$	0.781	0.317	-0.144
g_s^z/g_s	0.88 ± 0.04	a) 1.01 ± 0.02 b) 0.95 ± 0.09	a) 0.83 ± 0.02 b) 0.76 ± 0.03
g_s^+/g_s	0.37 ± 0.03	a) 0.60 ± 0.01 b) 0.64 ± 0.03	a) 0.39 ± 0.05 b) 0.51 ± 0.05

a) Without correction for Coriolis mixing

b) Corrected for Coriolis mixing with K = 3/2 band.

REFERENCES

1. The discovery was reported in:
R. L. Mössbauer, Z. Physik 151, 124 (1958);
R. L. Mössbauer, Naturwiss. 45, 538 (1958);
and R. L. Mössbauer, Z. Naturforsch. 14a, 211 (1959).
General references for the Mössbauer effect that the author has frequently consulted, and on which the Introduction is based, include:
A. Abragam, L'effet Mössbauer et ses applications a l'étude des champs internes (unpublished lecture notes);
Gunther Wertheim, Mössbauer effect: principles and applications (Academic Press, New York, 1964);
and Horst Wegener, Der Mössbauereffekt und seine Anwendung in Physik und Chemie (Bibliographisches Institut, Mannheim, 1965).

2. D. Agresti, E. Kankeleit, and B. Persson, Phys. Rev. 155, 1339 (1967) and Phys. Rev. 155, 1342 (1967). Preliminary reports of the work were given in B. Persson, E. Kankeleit, and D. Agresti, Bull. Am. Phys. Soc. 11, 772 (1966); D. Agresti, E. Kankeleit, and B. Persson, Bull. Am. Phys. Soc. 11, 771 (1966); B. Persson, D. Agresti, and E. Kankeleit, Bull. Am. Phys. Soc. 11, 911 (1966).

3. Nuclear Data Sheets B1-1.

3a. The values for α and β (of Equation I. 5) were obtained from Nuclear Data Sheets B1-1.

4. O. Glemser, H. Sauer, and P. König, Z. anorg. Chemie 257, 17 (1948).

5. P. Duwez, private communication.

6. E. Kankeleit, Rev. Sci. Instr. 35, 194 (1964); Mössbauer Effect Methodology Vol. 1, edited by I. Gruverman (Plenum Press, New York, 1965), p. 47.

7. S. S. Hanna, R. S. Preston, and J. Heberle, in The Mössbauer Effect, edited by D. M. J. Compton and A. H. Schoen (John Wiley & Sons, Inc., New York, 1962), p. 85.

8. For a recent compilation, see W. Ebert, O. Klepper, and H. Spehl, Nuclear Phys. 73, 217 (1965).

9. S. G. Nilsson and O. Prior, Kgl. Danske Videnskab Selskab, Mat.-Fys. Medd. 32, No. 16 (1961).

10. J. R. Harris, G. M. Rothberg, and N. Benczer-Koller, Phys. Rev. 138, B554 (1965).

11. F. K. McGowan and P. H. Stelson, Phys. Rev. 116, 154 (1959).

12. I. Lindgren, in Perturbed Angular Correlations, ed. E. Karlsson, E. Mathias, K. Siegbahn (North-Holland Publishing Co., Amsterdam, 1964), p. 399.

13. W. Gordy and W. J. O. Thomas, J. Chem. Phys. 24, 439 (1956).

13a. P. H. Barrett, R. W. Grant, M. Kaplan, D. A. Keller, and D. A. Shirley, J. Chem. Phys. 39, 1035 (1963).

14. E. A. Phillips and L. Grodzins, in Perturbed Angular Correlations, edited by K. Siegbahn (North-Holland Publishing Co., Amsterdam, 1964), p. 294.

15. S. V. Karyagin, Proc. Acad. Sci. USSR, Phys. Chem. Sect. 148, 110 (1964).

16. N. Sikazono, H. Takekoshi, and T. Shoji, J. Phys. Soc. Japan 20, 271 (1965).

17. E. Kankeleit, Z. Physik 164, 442 (1961); S. G. Cohen, N. A. Blum, Y. W. Chow, R. B. Frankel, and L. Grodzins, Phys. Rev. Letters 16, 322 (1966).

18. D. Bloess, A. Krusche, and F. Münnich, Z. Physik 192, 358 (1966).

19. W. M. Visscher, as quoted in H. Frauenfelder, The Mössbauer Effect (W. A. Benjamin Inc., New York, 1962), p. 45.

20. J. D. Bowman, E. Kankeleit, E. N. Kaufmann, and B. Persson, Nucl. Instr. & Methods, to be published.

21. E. Kankeleit, Bull. Am. Phys. Soc. 10, 65 (1965); the value has been recalculated using $g(2^+) = 0.24$.

22. Masaaki Kontani and Junkichi Itoh, J. Phys. Soc. Japan 22, 345 (1967).

23. F. Boehm, G. B. Hagemann, and A. Winther, Phys. Letters 21, 217 (1966) and G. Goldring, private communication.

24. B. Herskind, J. D. Bronson, R. R. Borchers, L. Grodzins, and D. E. Murnick, Bull. Am. Phys. Soc. 12, 503 (1967).

25. D. A. Shirley and G. A. Westenbarger, Phys. Rev. 138, A170 (1965).

26. L. A. Campbell, Proc. Phys. Soc. (London) 89, 71 (1966).

27. A. J. Freeman and R. E. Watson, in Magnetism, edited by G. T. Rado and H. Suhl (Academic Press, New York, 1965), Vol. II, Part A, Chap. 4, p. 167.

28. L. D. Roberts and J. O. Thompson, Phys. Rev. 129, 664 (1963).

29. American Institute of Physics Handbook (McGraw Hill Book Co., Inc., New York, 1963), 2nd ed., p. 5 - 170.

30. O. Hansen, M. C. Oleson, O. Skilbreid, and B. Elbek, Nuclear Phys. 25, 634 (1961).

31. O. I. Sumbaev, A. I. Smirnov, and V. S. Zykov, Soviet Phys. - JETP 15, 82 (1962).

32. A. K. Kerman, Kgl. Danske Videnskab Selskab, Mat.-Fys Medd. 30, No. 15 (1956).

33. D. J. Rowe, Nuclear Phys. 61, 1 (1965).

34. R. T. Brockmeier, S. Wahlborn, E. J. Seppi, and F. Boehm, Nuclear Phys. 63, 102 (1965).

35. B. Persson, H. Blumberg, and D. Agresti, submitted to Phys. Letters.

36. K. Kumar and M. Baranger, Phys. Rev. Letters 17, 1146 (1966).

37. W. F. Edwards, F. Boehm, J. Rogers, and E. J. Seppi, Nuclear Phys. 63, 97 (1965).

38. U. Gruber, R. Koch, B. P. Maier, and O. W. B. Schult, Z. Naturforsch. 20a, 929 (1965).

39. P. Alexander and R. S. Hager, Phys. Rev. 139, B288 (1965).

40. L. A. Sliv and I. M. Band in $\alpha \cdot \beta \cdot \gamma$ Ray Spectroscopy edited by K. Siegbahn (North-Holland Publishing Co., Amsterdam, 1965) p. 1639. The total internal conversion coefficient was estimated from $\alpha_t = 1.3\ \alpha_L$.

41. Z. Bochnacki and S. Ogaza, Inst. of Nuclear Physics, Cracow, Report No. 428/PL (1965); Z. Bochnacki and S. Ogaza, Nucl. Phys. 69, 186 (1965).

42. S. G. Nilsson, Private communication (June, 1966).

43. S. G. Nilsson, Kgl. Danske Videnskab Selskab, Mat.-Fys. Medd. 29, No. 16 (1955).

44. P. Sparrman, T. Sundström, and J. Lindskog, Arkiv Fysik 31, 409 (1966).

45. C. Günther and E. Kankeleit, Phys. Letters 22, 443 (1966).

46. W. Henning, P. Kienle, E. Steichele, and F. Wagner, Phys. Letters 22, 446 (1966).

47. A. Bohr and B. Mottelson, unpublished lecture notes on Nuclear Structure and Energy Spectra (Copenhagen 1962), Chapter V.

48. Z. Bochnacki and S. Ogaza, Acta. Phys. Polon. 27, 649 (1965).

49. M. Atac, P. Debrunner, and H. Frauenfelder, Phys. Letters 21, 699 (1966).

50. A. B. Buyrn and L. Grodzins, Phys. Letters 21, 389 (1966) and as quoted in Reference 53.

51. N. Benczer-Koller, J. R. Harris, and G. M. Rothberg, Phys. Rev. 140, B547 (1965).

52. A. de-Shalit, Phys. Rev. 122, 1530 (1961).

53. A. Gal (Braunstein), Phys. Letters 20, 414 (1966).

54. Y. K. Agarwal, C. V. K. Baba, and S. K. Bhattacherjee, Nucl. Phys. 79, 437 (1966).

55. L. Keszthelyi, I. Berkes, I. Deszi, and L. Pocs, Nucl. Phys. 71, 662 (1965).